The Effects of Magnetic Dilution and Applied Pressure on Several Frustrated Spinels

by

Jory T. Korobanik

B.Sc. (Honours) Physics, Department of Physics, Brock University, 2009

A THESIS SUBMITTED IN PARTIAL FULFILMENT OF
THE REQUIREMENTS FOR THE DEGREE OF

DOCTOR OF PHILOSOPHY

in

The Faculty of Mathematics and Sciences

Department of Physics

BROCK UNIVERSITY

February 21, 2016

In presenting this thesis in partial fulfilment of the requirements for an advanced degree at the Brock University, I agree that the Library shall make it freely available for reference and study. I further agree that permission for extensive copying of this thesis for scholarly purposes may be granted by the head of my department or by his or her representatives. It is understood that copying or publication of this thesis for financial gain shall not be allowed without my written permission.

(Signature) _____

Department of Physics

Brock University
St.Catharines, Canada

Date _____

Abstract

The effects of magnetic dilution and applied pressure on frustrated spinels $GeNi_2O_4$, $GeCo_2O_4$, and $NiAl_2O_4$ are reported. Dilution was achieved by substitution of Mg^{2+} in place of magnetically active Co^{2+} and Ni^{2+} ions. Large values of the percolation thresholds were found in $GeNi_{2-x}Mg_xO_4$. Specifically, $p_{c1} = 0.74 \pm 0.04$ and $p_{c2} = 0.65 \pm 0.05$ in the sub-networks associated with the triangular and kagomé planes, respectively. This anomalous behaviour may be explained by the kagomé and triangular planes behaving as coupled networks, also know as a network of networks. In simulations of coupled lattices that form a network of networks, similar anomalous percolation threshold values have been found. In addition, at dilution levels above $x = 0.30$, there is a T^2 dependency in the magnetic heat capacity which may indicate two dimensional spin glass behaviour. Applied pressures in the range of 0 GPa to 1.2 GPa yield a slight decrease in ordering temperature for both the kagomé and triangular planes.

In $GeCo_{2-x}Mg_xO_4$, the long range magnetic order is more robust with a percolation threshold of $p_c = 0.448$. Similar to diluted nickel germanate, at low temperatures, a T^2 magnetic heat capacity contribution is present which indicates a shift from a 3D ordered state to a 2D spin glass state in

the presence of increased dilution. Dynamic magnetic susceptibility data indicate a change from canonical spin glass to a cluster glass behaviour. In addition, there is a non-linear increase in ordering temperature with applied pressure in the range $P = 0$ to 1.0 GPa.

A spin glass ground state was observed in $Ni_{1-x}Mg_xAl_2O_4$ for ($x = 0$ to 0.375). Analysis of dynamic magnetic susceptibility data yield a characteristic time of $\tau_* = 1.0 \times 10^{-13}$ s, which is indicative of canonical spin glass behaviour. This is further corroborated by the linear behaviour of the magnetic specific heat contribution. However, the increasing frequency dependence of the freezing temperature suggests a trend towards spin cluster glass formation.

Contents

List of Tables

List of Figures

Acknowledgements

I would like to thank everybody who helped me along my long and winding path. Without them I would have never gotten this far. In particular, I want to thank my mother Deborah and my grandmother Jeanne for all their personal and financial support. You stuck with me for as long as I needed and never lost faith in me. I thank my brothers Mario, Collin, and Chris who make me very proud. I thank Ducky and Moomoo who often sat with me during the writing process. Also, I thank all my friends and the faculty and staff in the department of physics.

I wish to thank Kevin Caslin for taking the x-ray diffraction measurements for CGO and NAO. I also appreciated the discussions we had regarding this work and Rocksmith jam sessions. In addition, I thank Patrick Reuvekamp for his training, guidance, friendship, and the excellent strain measurements for NGO. Also, without your help I'd probably still be stuck in the Stuttgart airport.

I would like to thank my supervisor Dr. Razavi for sticking with me throughout the years. Not only have you taught me about experimental physics, you have taught me to be a more compassionate and worldly person.

I thank Leslie Nash for all of her support and motivation throughout the last 5 years. I would have never made it without you. You helped me through the most difficult times.

Lastly, I want to dedicate this work to the memory of Michael Paul Rolo. I miss you and think about you all the time.

Chapter 1

Introduction

Disordered materials are part of our everyday life. For example, the glass cup we drink out of, many plastics, and the eggs we eat for breakfast are examples of structurally disordered materials. In these systems, there is little to no correlation in the spatial distribution of their basic building blocks. As a consequence, there is a lack of translational symmetry and periodicity. The most successful theories of solids utilize periodicity and symmetry as starting points are, just to mention a few, reciprocal lattice, Bloch's theorem, and diffraction. Progress in understanding disordered, glassy and ill-condensed systems has been slow. For example, researchers still strive to adequately explain why structural glasses are rigid. The standard arguments for generalized rigidity [1] seem to fail for these materials. [2] This knowledge gap, among others, is one of the features that make research in glassy and disordered systems interesting. Furthermore, a strong argument can be made that glasses fall under the umbrella of complex systems. This constitutes an emerging field where physicists, mathematicians, ecologists, social scientists, and financial engineers could work together to solve fascinating problems.

To simplify matters, researchers could study disordered systems by shifting the disorder from the structure to other system parameters such as magnetic moments and electric dipoles. In this way, many of the familiar tools that physicists and material scientists use to describe ordered solids, are available. From an experimental perspective, this means working with materials that form crystals with a network of stable, well defined, repeating units. This is contrasted to systems, such as window glass, where disorder is structurally "built in". With the decoupling of structure and disorder, one is free to not only select the type of disorder on the network (lattice), but also vary the amount of it present in the material. For example, a three dimensional network of magnetic ions can be perturbed by dilution: the act of replacing a magnetically active ion with a non-magnetic one, while retaining the overall crystal structure. By varying the dilution level, one can monitor certain characteristics of the magnetic network such as the stability of the long range

order state (transition temperature) and the nature of the magnetic ground state (anti-ferromagnetic, spin glass, etc).

This work seeks to understand the effects of magnetic dilution and applied pressure on GeM_2O_4 (M = Ni, Co) and $NiAl_2O_4$[1]. The magnetic ground state of GeM_2O_4 (M = Ni, Co) is characterized by two alternately stacked, crystallographically distinct, ordered planes with triangular motifs. [3, 4, 5] To produce this ordered state, a long range exchange network with interactions up to the fourth nearest neighbours J_4 has been suggested. [6, 5] Although these compounds have the same low temperature magnetic state, the way in which magnetic order manifests itself, is very different for each material. In $GeCo_2O_4$, the stacked planes order simultaneously. Conversely, in $GeNi_2O_4$, each planar type has its own distinct purely magnetic transition temperature. [7] Given these similarities and differences, the main focus is to understand, compare, and contrast how the ordered magnetic ground states of $GeNi_2O_4$ and $GeCo_2O_4$ evolve with the perturbative effects of magnetic dilution and applied pressure. This is of interest due to the intricate exchange network required to produce this unique low temperature state. Attention is paid to the robustness of the magnetic long range order and the nature of the magnetically diluted state. Regarding $NiAl_2O_4$, the magnetic ground state is currently unknown. Motivation for this compound stems from the placement of Ni^{2+} ions, that reside in a complimentary sub-lattice, which will be further discussed in Section 1.1.

Magnetic dilution is a useful tool to better understand a system's low temperature state and the importance of exchange interactions. It is widely used to probe materials that exhibit magnetic frustration to determine the effects of quenched disorder, in the presence of frustrated magnetic interactions [8], which can often lead to spin-glass behaviour. [9, 10] Even in non-frustrated materials, dilution beyond a critical level causes a phase transition, which is often described using percolation theory (see section 2.0.7). [11] If the non-magnetic ion has the same oxidation state and approximately the same ionic radius, dilution should not have a major effect on the crystal lattice size due to chemical pressure, which can arise from spatial differences between native and doped ion. [12] This is important if one wishes to isolate effects from changes that are driven by shifts in lattice parameter. A more direct way to probe lattice size effects, with respect to lattice shrinkage, is to use applied pressure. This has been shown to induce substantial changes in the physi-

[1] Only dilution was completed on $NiAl_2O_4$

cal properties. For example, applied pressure relieves frustration in the spin liquid $Ho_2Tb_2O_7$, causing it to order antiferromagnetically approximately at $P = 2$ GPa. [13]

The magnetic behaviour of the materials studied in this thesis is driven by the spinel-type crystal structure, which gives rise to the planar nature of the magnetic ground state of the germanate compounds. [14] In the following sections, magnetic frustration, and the structure of these compounds will be explained, followed by a deeper introduction to the compounds studied in this thesis, to further motivate the research.

1.0.1 Frustration

The term frustration, in the microscopic sense, characterizes a system with competing interactions that cannot be simultaneously satisfied. [15] Much interest has been generated in frustrated materials as they have been shown to have a variety of unique ground states such as spin glasses [16, 10, 17] and spin ices. [18] Early theoretical work by Wannier [19] on an antiferromagnetic triangular Ising net revealed that the system has no ordering temperature. Later in the 1970s, physical manifestations of frustration were found in the dilute alloys $Cu_{1-x}Mn_x$ and $Au_{1-x}Fe_x$ which form spin glasses, a metastable ground state without long range magnetic order distinguished by a well defined freezing temperature T_f. [16] Spin glass materials require [9] both frustration and randomness.[2] In these alloys, frustration and randomness are coupled as they are brought on by the stochastic placement of the magnetic impurities (Mn,Fe). The magnetic interaction between the chaotic placement of impurity sites is of RKKY type, whose sign and strength oscillates with ion separation distance (see equation 2.5). [9] Interest in the sole effect of frustration requires the decoupling of frustration and disorder. This is accomplished by selecting nets or lattices that exhibit frustration strictly due to their symmetry, simply known as geometric frustration. [21]

Geometric frustration is often[3] found on triangular-type lattices with AFM exchange. Figure 1.1 illustrates this concept simply as the right "spin" can not satisfy the AFM interaction for both neighbours. Two of the spins are energetically satisfied with the final spin direction ill-determined due

[2]Some authors use the term "disorder" [20] instead of "randomness". [10] I prefer "randomness" and reserve "disorder" for the collective behaviour of a phase.

[3]Frustration can be found in many lattices such as square and one dimensional linear chains if next nearest neighbour interactions are included.

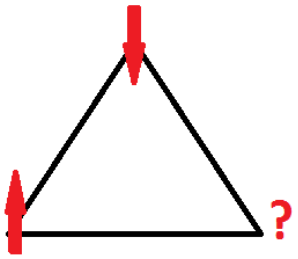

Figure 1.1: Illustration of geometrically frustrated AFM Ising triangle with right-most spin direction ambiguous.

to both configurations having the same configuration energy. Specifically, regardless of direction the system has one neighbour unsatisfied. This ambiguity of the minimum energy configuration increases the ground state degeneracy which, in the thermodynamic limit for large systems, becomes an extensive quantity [22] and scales with system size. Examples of geometrically frustrated lattices in two dimensions are edge sharing and corner sharing (kagomé) lattices. Three dimensional extensions of these are the pyrochlore type and spinel type structures, which highlight their frustration when viewed along particular axes. [15] Magnetic frustration can also occur in polygonal single molecular magnetics.[23] Experimentally, frustrated materials exhibit strikingly different magnetic behaviour compared to non-frustrated antiferromagnets. For example, regular AFM materials obey the Curie-Weiss law (equation 2.6) above their transition temperature, with a negative Weiss constant θ_{cw} whose absolute value yields the Néel ordering temperature. Frustrated systems also obey the same model except that the actual ordering temperature is lower than the predicted θ_{cw} value. [17] Put simply, geometric frustration quenches Néel ordering. In fact, to characterize the strength of frustration often one uses the frustration parameter [9] $f = |\theta_{cw}|/T_n$ which is a measure of the level of Néel Suppression ($f > 10$ is considered a highly frustrated material). Since the dominant magnetic contributions to the Hamiltonian, the nearest neighbour spin interactions, are at odds with each other in frustrated materials, the ground state is often selected by small corrections such as next nearest neighbour interactions, dipole interactions, and structural distortion. [14]

1.1 Spinel Structure

Motivation for selecting materials with spinel structure (AB_2X_4) stems from its stability, ability to accept many d-series ions, allowing many different oxidation states, and its manifestation of strong geometrical frustration. [15, Ch. 6] These characteristics of materials within the spinel family of structures give rise to a rich and diverse catalogue of low temperature magnetic states. [15, Ch.7]

Chemically, the spinel structure is rather accommodating, with many different combinations of transition metal ions available. The variation is further enhanced due to O, Se, and S allowed for the ligand X. Oxides tend to be insulating while sulphides generally have better conductive properties due to better overlap of the p and d orbitals between ligand and metal ion. [15, Ch.6] Furthermore, there are a number of common oxidation states that are found in these compounds such as $A^{1+\rightarrow 4+}$ with corresponding $B^{2+\rightarrow 4+}$. To signify oxidation state, two numbers are given to represent the A and B site metal ion oxidation state respectively. For example, a 2-3 spinel type compound has $A^{2+}$and B^{3+}.

To fully characterize a compound, that has a cubic spinel structure, one must provide lattice parameter (a), inversion parameter (x), and oxygen parameter (u). [24] Inversion describes the tendency for A site ions to swap places with B sites ions. A spinel is called normal if the metal ions reside in their "proper" location and inverse if the metal ions fully swap places. This defect is important in some materials such as $CoAl_2O_4$ which affects the nature of its magnetic ground state. Careful heat treatments during synthesis has been shown to minimize inversion (see section 1.2.3). [25] The oxygen parameter describes the distortion the octahedrally coordinated O^{2-} ions that surround the B sites. A value of $u = 0.375$ is considered undistorted. A larger u indicates a reduction of the octahedra and a corresponding expansion of the A site tetrahedra. The converse occurs when u is smaller than 0.375. In both cases, the symmetry of the tetrahedra remains while the octahedra skew which reduces their symmetry. This effect can have an important effect on electronic states for d-series ions. [24, 15]

The spinel structure is generated by tetrahedral AX_4 and octahedral BX_6 which can naturally be divided into two distinct sub-lattices. The B sites themselves are arranged in three dimensional corner sharing tetrahedra.

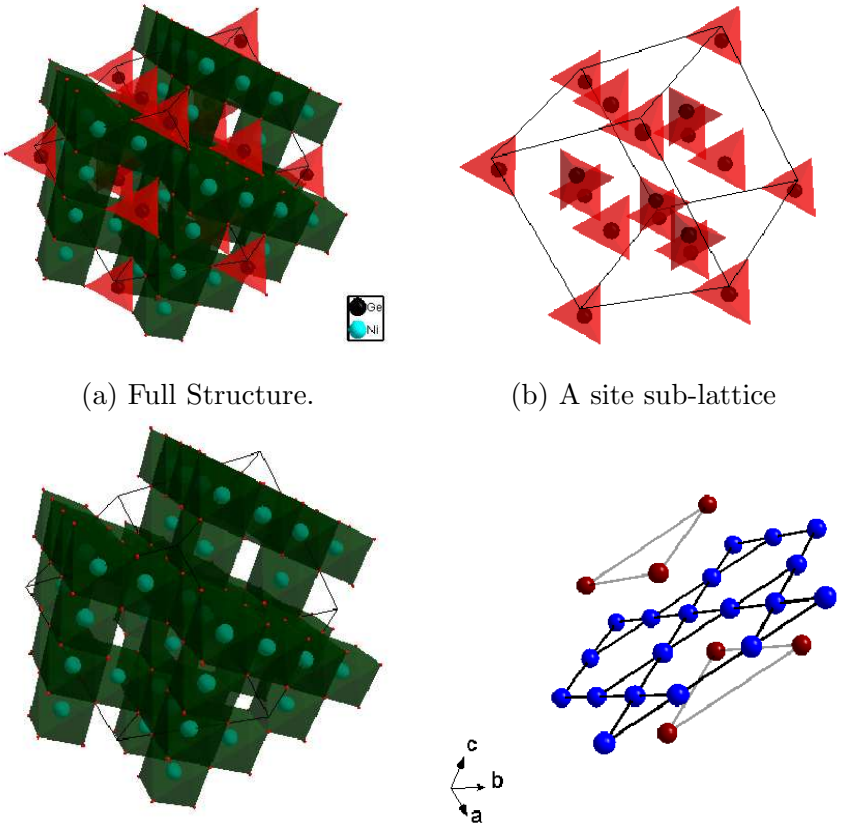

(a) Full Structure. (b) A site sub-lattice

(c) B site sub-lattice (d) Planar structure of B-sites.

Figure 1.2: Illustration of the cubic spinel-type structure:(A) Full structure of $GeNi_2O_4$ with Ge^{4+} ions in (red) tetrahedral coordination with O^{2-} and octahedral coordination (green) of Ni^{2+} with O^{2-}. (B) A site sub-lattice which has a diamond structure. (C) B site sub-lattice which is constructed by corner sharing tetrahedra (in this case Ni^{2+} ions). Due to the similarity of corner sharing tetradedra found in pyrochlore materials, this sub-lattice is often termed "pyrochlore". (D) B sites form alternating stacked layers of kagomé (blue spheres) and triangular planes (red spheres), which can generate strong geometric frustration.

This is the same sub-lattice that is found in pyrochlore $A_2B_2O_7$ compounds[4]. When viewed along the [111] direction, these corner sharing tetrahedra appear as an alternate stacking of triangular and kagomé planes. In fact, the stack of kagomé-triangular-kagomé (K-T-K) is quite ubiquitous and is often called a kagomé sandwich or pyrochlore slab. [26, 27] When the B sites contain magnetic ions, the system can exhibit strong geometrical magnetic frustration due to the corner sharing and edge sharing triangles that make up the kagomé and triangular planes, respectively. [21] The sub-lattice associated with the A sites in the spinel has a diamond type structure. One would expect this configuration to not exhibit any magnetic frustration effects when occupied by magnetic ions. However, there are several examples of frustrated materials, such as $FeSc_2S_4$ [28] and MAl_2S_4 (M=Co, Fe, Mn) [29], whose magnetic character arises from the diamond A site sub-lattice. All of these properties are important reasons for the diverse low temperature states found in materials that crystallize in the spinel structure.

The stacked kagomé and triangular planes that are the building blocks of the B sub-lattice, found in spinel-type materials, are not the only arrangement available. There are several interesting structures, related to spinels, that contain these planar structures in different layering regimes. An important structure, in the context of this thesis, is the magnetoplumbite $SrGa_{12-x}Cr_xO_{19}$ (SCGO(x)). This compound is a highly frustrated system ($f = 117$) that is formed by the K-T-K kagomé stack connected by two non-frustrated linking layers. [30] This material behaves as a spin-glass[31] in the range $1 \leq x \leq 9$ and neutron diffraction experiments indicate that spins in the linking layers form spin dimers. [26] This segmentation of the kagomé sandwich results in strong 2D character which is attributed to an unusual quadratic temperature dependence in the magnetic specific heat at low temperatures. [32, 33] This contrasts the expected linear behaviour of the magnetic specific heat that is found in canonical spin glasses. [17, 10]

1.2 Introduction To Materials Studied

This section is dedicated to describe the materials that will be studied in this thesis and to better motivate the research undertaken. It will also review previous work that has been completed and highlight some of the outstanding questions that remain to be answered regarding their physical properties.

[4] In pyrochlores, the two sub-lattices that are formed by A sites and B sites are identical.

Following this, Chapter 2 will focus on a review basic aspects of magnetism in insulating oxide compounds, Chapter 3 will describe the experimental methods. The remaining chapters are dedicated to the experimental results obtained, followed by a discussion, and conclusion.

1.2.1 $GeNi_2O_4$

$GeNi_2O_4$ (NGO) crystallizes in a cubic spinel structure type AB_2O_4 with A=Ge^{4+} and B=Ni^{2+}. When Ni^{2+} sites are diluted with Mg^{2+} an olivine structure can form as an impurity above a critical concentration. [34] This effectively puts an upper limit on the Mg^{2+} concentration at approximately 60% unless high pressure synthesis techniques are used. [34] As discussed above, materials that crystallize with a spinel structure (AB_2O_4) are composed of octahedrally coordinated B sites and tetrahedrally coordinated A sites. One can view this structure as two interpenetrating diamond and pyrochlore sub-lattices that are associated with either the A site (diamond) or B site (pyrochlore) which is illustrated in Figure 1.2a. When viewing the B sub-lattice along the [111] direction one observes alternate stacking of kagomé and triangular planes which is highlighted in Figure 1.2d. The degeneracy of 3d orbitals for Ni^{2+} ions ($^3F_4$) in octahedral crystal electric field (CEF) is lifted with a ground state of S=1. In addition, there is also a small trigonal CEF field which further splits the t_{2g} level into a singlet and doublet with the doublet having lower energy. Spin orbit coupling further splits these levels, but can be ignored in the temperature region studied here. [7, 35]

Interest in $GeNi_2O_4$ has grown due to the existence of two closely spaced magnetic transitions, shown in Figure 1.3, at $T_{N1} = 12.0$ K and $T_{N2} = 11.4$ K with a Curie-Weiss[5] temperature of 15K. [3] Neutron diffraction studies [5] yield a $\mathbf{Q} = (1/2, 1/2, 1/2)$ propagation vector indicating that these ordering phenomena are due to alignment of spins within the stacked kagomé and triangular planes. Specifically, at T_{N1} the spins within the kagomé planes align ferromagnetically with antiferromagnetic alignment between successive like-planes. At T_{N2} the triangular planes arrange themselves in the same fashion. This is further corroborated by implanted muon experiments which indicate two distinct local magnetic environments that can be interpreted as the kagomé and triangular planes. [36] Magnetic measurements in high fields

[5]There is an appreciable variation of the value of the T_{CW} which will be discussed in Chapter 4.

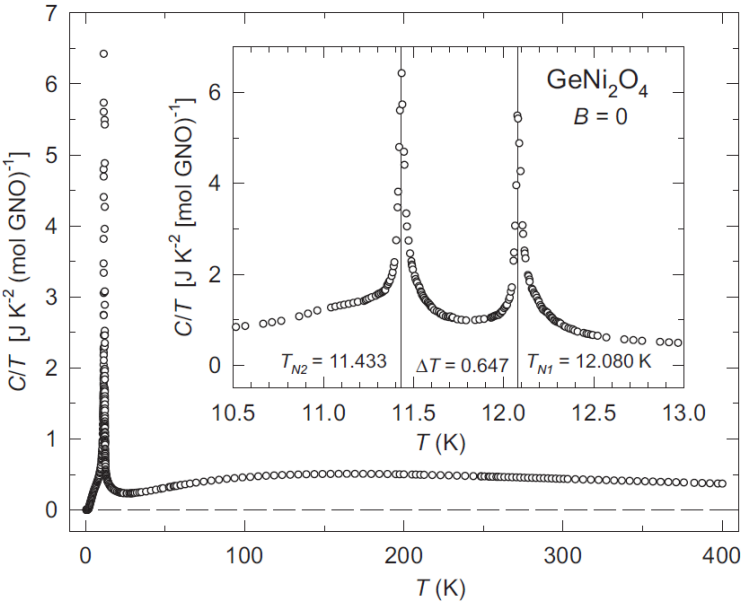

Figure 1.3: Reproduced from Lashley *et al.* [7]. Illustration of the distinct AFM transitions observed in the specific heat data for NGO at B=0.

on polycrystalline samples reveal two spin-flop transitions at $H = 30$ T and $H = 37$ T. [5] To model this ordering behaviour, a large exchange network with a large fourth nearest-neighbour J_4 term is required. [6] The nearest neighbour J_1 term is weak due to a 90 degree Ni-O-Ni bond angle. [37] Furthermore, neutron data and analysis of specific heat [3, 7] data indicate the presence of non-gapped AFM spin waves and a gapped excitation with an energy of approximately 10.8 K. Although triangular and kagom'e systems have the ability to exhibit strong frustration, NGO does not exhibit appreciable Néel quenching as the frustration parameter is approximately $f = 1.25$. This is possibly due to the interplanar interactions being FM with frustration arising from the addition of further nearest neighbour interactions as is found in Al_2MO_4 (M = Mn, Co, Fe). [29]

The realization of two distinct magnetic transitions is not unique to NGO. $CsNiCl_3$ (S=1) is a stacked triangular layered compound that undergoes two magnetic transitions but has strong one dimensional behaviour. [38, 39]. Specific heat results for $CsNi_{1-x}Mg_xCl_3$ for x=0.02 indicate both transitions are still present albeit lowered by approximately 0.2 K. [40] A more fitting com-

parison can be made with the Heisenberg pyrochlore $Gd_2Ti_2O_7$ (GTO) which shares the same sub-lattice as the Ni^{2+}. However, neutron diffraction studies using $^{160}Gd^{3+}$ (due to neutron absorption issues) indicate that the magnetic ground state is related but not equivalent to NGO as it lacks planar structure. [41]

Specific heat data for NGO have shown that only approximately 60% of the expected magnetic entropy is recovered. In addition, the entropy change associated with each ordering event is nearly the same which is unusual as three times as many spins reside on the kagomé compared to the triangular planes. [7]

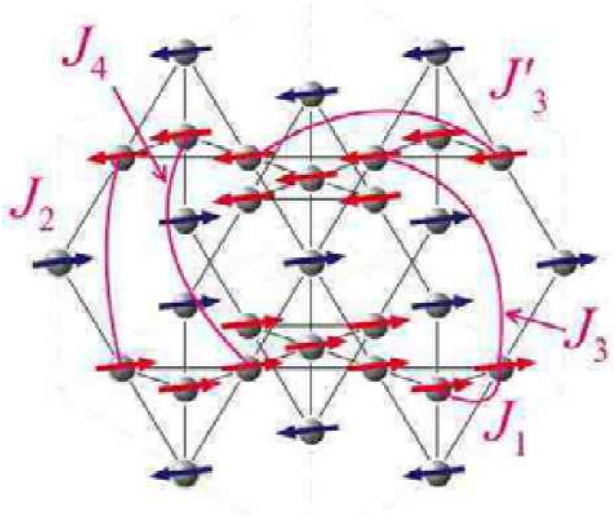

Figure 1.4: Reproduced from Matsuda *et al* [6]. Illustration of the exchange network up to fourth nearest neighbours for an ion residing in the triangular plane. Red and blue arrows indicate a kagomé and triangular sites respectively.

The ordered state of NGO can be thought of two distinct crystallographic lattices (kagomé and triangular) that are coupled together due to high order exchange. This makes NGO an excellent candidate to perturb the network of exchange interactions that create this unique ground state. An illustration of this network of neighbours is given in Figure 1.4. An interesting feature is that each plane type has a different nearest neighbour profile. For example, 4 of 6 nearest neighbours of an ion in a kagomé plane lie within its plane. Conversely, none of nearest neighbours of a triangular site are intraplanar,

they all lie on kagomé sites. We seek to understand the implications of magnetic dilution with Mg^{2+} ions on each layer type individually and how disorder permeates the system as a whole.

1.2.2 $GeCo_2O_4$

Similar to NGO, $GeCo_2O_4$ (CGO) crystallizes in a cubic spinel structure with Co^{2+} ($3d^7$: L=3, S=1) occupying the B site sub-lattice.[4] This sub-lattice can be viewed as an alternating stack of triangular and kagomé planes. In an octahedral crystal electric field the L=3 state splits to form an L=1 lowest energy level. Spin-orbit coupling separates this level into J = 1/2, 3/2, and 5/2 with 1/2 having the lowest energy. A trigonal CEF at the Co^{2+} site further splits this three levels into 6 Kramer's doublets with energy levels: 0, 180, 360, 440, 1760 and 1030 Kelvin. [7] These levels have a significant contribution to the magnetic and specific heat and must be factored in to obtain meaningful results.

Early work on $GeCo_2O_4$ [24, 4, 7] revealed an applied magnetic field dependent antiferromagnetic transition at T_n=20.6 K. It is not possible to extract relevant Curie-Weiss constants from linear fits due to the contributions from thermally accessible crystal field levels, although several values were reported. [4, 42] The shape of the specific heat anomaly suggested that there is a concurrent cubic to tetragonal lattice distortion (c/a=1.001) that occurs at this transition. Below T_n gapped AFM spin waves exist with an associated energy of 38.4 K. [7] This was confirmed in inelastic neutron experiments which set the gap energy at 35 K. [7]

The exchange network for is believed to be the same as NGO but with the addition of a FM direct exchange term between Co^{2+} ions. [37] In addition, the low temperature magnetic state of CGO has the same structure as NGO: FM alignment within each triangular and kagomé planar type with AFM alignment between like planes which yields overall AFM order. [5, 37] Contrasting with NGO, both planar types order simultaneously which may be due to the observed structural effects at T_n. [7] Neutron diffraction experiments in large applied fields have revealed three distinct magnetic phases: Phase one (0 - 4 T): AFM alignment between similar triangular and kagomé planes, Phase two (4 - 10 T): FM alignment between triangular planes while kagomé retain AFM, Phase Three (above 10 T): all planes are in FM alignment. [37]

Recently, the interplay between the structural effects and the magnetic

behaviour were investigated carefully. Barton *et al* used synchrotron x-ray diffraction data taken below 24 K and observed structural events at T = 20.6 K and 16 K. At the ordering temperature, there is a small lattice shrinkage due to magneto-restriction, not a shift from cubic to tetragonal as originally believed to occur. Interestingly, the structural transition actually occurs at 16 K, which does not coincide with magnetic ordering and is suggested to stem from Jahn-Teller distortion. [43]

In this study, the effects of magnetic dilution and applied pressure on $GeCo_2O_4$ are determined. Dilution is achieved by randomly replacing Co^{2+} ions with non-magnetic Mg^{2+}. Of interest is how the planar magnetic structure will respond to the random placement of Mg^{2+}. Several question can be asked: will the magnetic ordering of the triangular and kagomé planes still occur simultaneously with random dilution? How does the dimensionality of the magnetic state evolve with increased dilution? What is the percolation threshold for this system? In light of the observed structural distortion in CGO, how will applied external pressures manifest itself? Lastly, how do all of these compare to NGO?

1.2.3 $NiAl_2O_4$

$NiAl_2O_4$ crystallizes in a cubic spinel type structure with a lattice constant a=8.0461 Å. The B site contains a non-magnetic Al^{3+} ion and a magnetically active Ni^{2+} ion residing on the diamond type A sub-lattice. Research on this compound has focussed on structural and its catalytic properties. The specific heat of was measured and an lambda anomaly was found at 7.5 K. [44] To the author's knowledge, no magnetic data are currently reported in literature.

This work on $NiAl_2O_4$ is motivated by magnetic studies in other magnetically active A site spinel type compounds such as $FeSc_2S_4$ and MAl_2O_4 where (M = Fe, Co, Mn). [29, 25] These materials exhibit geometrical frustration even though there are no magnetic ions residing on the B site. The origin of this frustration is AFM exchange across next nearest neighbours (NNN) and next-next nearest neighbours (NNNN) which appear as triangular units [29] that are illustrated in Figure 1.5. For this family of compounds special attention must be given to synthesis as small amounts of cation inversion produces completely different low temperature magnetic states. For example, early work indicated a spin-glass transition in $CoAl_2O_4$. [29] When site inversion is minimized, this material actually has a colinear AFM low

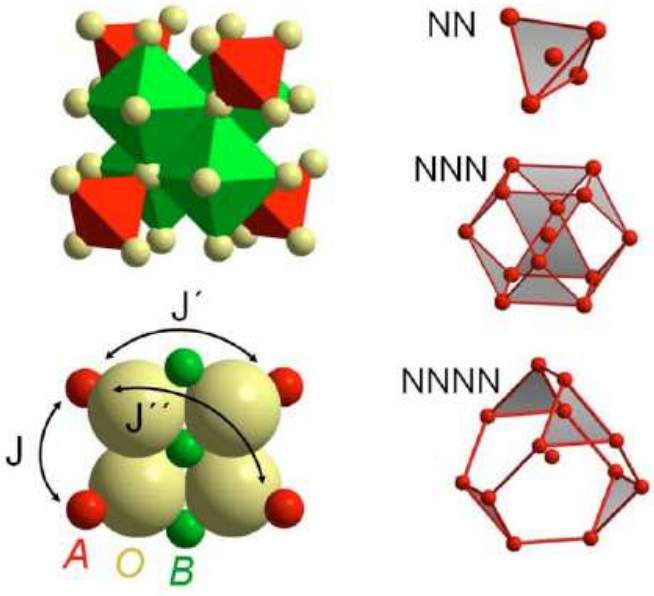

Figure 1.5: Magnetic exchange network in frustrated A-site spinels Reproduced from Tristan *et al* [29]. Illustration of the exchange network of the A-site diamond sub-lattice found in spinel-type structures.

temperature state. [25]

Chapter 2

Magnetism in Insulating Oxides

Magnetic behaviour stems from the angular momentum of charged particles which gives rise to magnetic moments. The scaling factor between moment μ and angular momentum $\mathbf{L}$ is known as the gyromagnetic ratio γ and can take different values. The resulting magnetic moment is given by

$$\boldsymbol{\mu} = \gamma \boldsymbol{L} \,. \tag{2.1}$$

There are two forms of angular momentum for electrons: an orbital component and a spin component. The orbital component arises from an electron's movement about the nucleus and is characterized by the usual quantum numbers ℓ and m_ℓ. Similarly, we have $s = 1/2$ and $m_s = \pm 1/2$ for the electron intrinsic spin component. In a many electron system under Russel-Saunders coupling[1], the spin and orbital momenta combine to form L and S. The total angular momentum vector $\mathbf{J} = \mathbf{L} + \mathbf{S}$ whose eigenvalue[2] can be expressed as $\sqrt{J(J+1)}$ with possible J values of (|L-S| $\leq J \leq$ L+S). The magnetic moment that is created by J is given by

$$\boldsymbol{\mu_J} = g_L \mu_B \boldsymbol{J} \quad \text{where,} \qquad g_L = \frac{3}{2} + \frac{(S+1) - L(L+1)}{2J(J+1)} \tag{2.2}$$

and g_L is the Landé g factor. In a many electron ion there are several ways to combine the spin S and orbital L terms. Hund's rules can be used in most cases to determine the lowest energy state in absence of crystal field effects, which are very important for d-shell ions. It utilizes the coupling effect between the electron spin moment and the apparent orbital motion of the nucleus around the electron, known as spin-orbit coupling.

[1] In Russel-Saunder coupling (L-S coupling) the spin-orbit interaction is weak. This applies to ions with small Z

[2] Rather, the eigenvalue for $\mathbf{J}^2$ is J(J+1)

2.0.4 Spin Orbit Coupling

Spin-orbit coupling describes how spin and angular momenta of an electron interact. The mechanism for the coupling of an electron's intrinsic spin and angular momentum arises from the apparent orbital motion, from the electron's frame of reference, of the positively charged nucleus. This "motion" of positive charge creates a magnetic field that interacts with the electron spin. The strength of this effect depends scales approximately as Z^4 making it important for the f block ions and to a lesser degree 4d and 5d transition metals. Regarding the 3d series of transitions metal ions, the strength of spin-orbit coupling is diminished due to a lower Z value. In addition, the d orbitals are more spatially spread out from the nucleus making electrostatic effects from neighbouring atoms in the solid more important.

2.0.5 Crystal Field Effects

The magnetic ground state of a free ion is set by spin-orbit coupling. When an ion is found within an ordered solid the surrounding ions create an electric field that depends on the symmetry of the lattice structure. This crystal electric field (CEF) causes some electron orbitals, which were all degenerate, to become energetically unfavourable due to electrostatic repulsion. The free ion orbital degeneracy is lifted and a new ground state is selected that depends on whether it is placed in a octahedral or tetrahedral environment which are common arrangements in oxides. In 3d ions, the five degenerate orbitals split into e and t_2 levels with e having lower energy in tetrahedral environment. In octahedral environments, t_{2g} level has lower energy (see figure 2.1). Another crystal field effect that is apparent in 3d ions is orbital quenching. Experimental values of $p_{eff} = g_L(J(J+1))^{1/2}$ for the iron series indicate that the orbital component is zero or near zero.

It is clear that the free ion picture needs several additions to make it reasonable for magnetic ions in the solid state. The relative size of the energy contributions of spin-orbit coupling versus crystal electric field dictate the overall energy level splitting. For most[3] 3d block ions,the crystal electric field energy is much larger than spin-orbit coupling. This results in the effects described above: splitting of free ion levels and orbital quenching. Once

[3]Particularly for Co^{2+}, the energy contributions from spin-orbit and CEF are comparable. There is still a significant orbital character due to incomplete orbital quenching. Please see the chapter on $GeCo_2O_4$ for more detail.

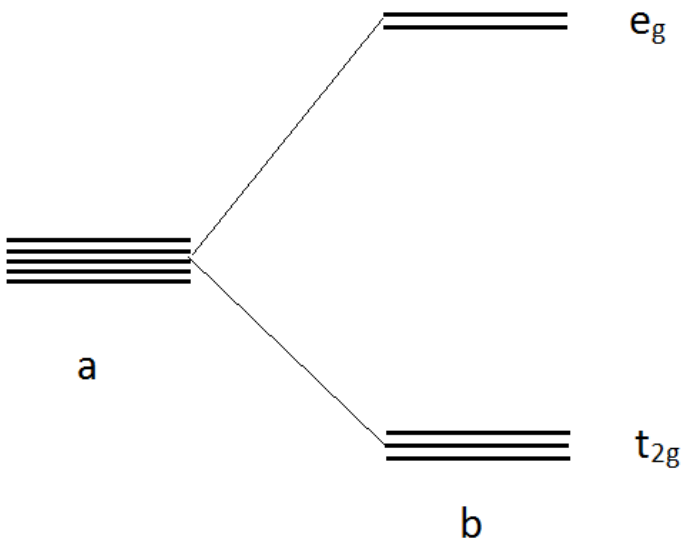

Figure 2.1: Crystal electric field effect on the electronic states of a 3d ion: (a) represents the free ion electronic state with degenerate levels. The right hand side represents the splitting of energy levels in an octahedral crystal electric field.

CEF effects are applied, spin orbit coupling can be applied as a perturbation which results in a further splitting which is only important at temperatures approximately below 1 K.

2.0.6 Interactions Between Spins

Dipole-Dipole Interaction

Once magnetically active ions are assembled into a solid they interact with each other which leads to emergent behaviour. The collection of electrons that reside on each ion can be treated as a single unit with a particular value of total spin J. The simplest and weakest interaction is dipole-dipole interactions. They are too small to cause an ordering event but become important at very low temperatures and in high spin systems. The energy

contribution of this can be approximated by

$$E_{dip} \approx \frac{\mu_0}{4\pi r^3} \left(\mu_1 \cdot \mu_2 - O(1/r^3) \right) . \tag{2.3}$$

Exchange

The most important mechanism for neighbouring spins to couple is through exchange and is a result of electrostatic interactions and the Pauli exclusion principle. The result is the celebrated Heisenberg equation

$$H = \sum_{<i,j>} J_{i,j} \boldsymbol{S_1} \cdot \boldsymbol{S_2} \tag{2.4}$$

where the exchange constant $J_{i,j}$ characterizes the strength and nature and the sum is over distinct neighbouring sites. There are many types of exchange: direct, superexchange, double exchange, etc. Direct exchange occurs through the direct overlap of wave functions from neighbouring ions. Clearly, there is a requirement for the orbitals to have a large radial distribution. This occurs to some degree in 3d metals, but not in the f block ions, where the f orbitals are much closer to the nucleus so no substantive overlap exists.

In oxides, there is no appreciable overlap of electron wave functions. Therefore an alternative medium of exchange is required to describe magnetism in these materials which is known as superexchange. For example in oxides, metal ions are surrounded by oxygen ions and connected in such a way that one can see a linkage of M-O-M-O-M (M=metal ion, O=oxygen ion). The driving mechanism is the energetic savings of de-localizing electrons on the metal ion by hopping to others along the connecting oxygen's p bonding orbitals. This exchange type is often antiferromagnetic but can be ferromagnetic. In addition, it is sensitive to the M-O-M bond angles in the determination if it is ferromagnetic (FM) or anti-ferromagnetic (AFM).

In metallic compounds, the free electrons can mediate a form of exchange called the Ruderman-Kittel-Kasuya-Yosida (RKKY) interaction given by

$$J_{RKKY} \propto \frac{cos(k_f r)}{r^3} . \tag{2.5}$$

The first spin glass materials discovered, which were dilute magnetic alloys, were the result of the RKKY interaction. The physical basis for this exchange interaction is caused by the polarization of electrons around Magnetic ions.

It is long ranged and J_{RKKY} is oscillatory with distance from the magnetic site.

Ordering and Critical Behaviour

Without exchange, spins are essentially[4] free and point in random direction and align in the direction of an applied magnetic field. This is known as the paramagnetic state. When exchange interactions are present, magnetic systems can undergo phase transitions, at well defined ordering temperatures T_c, to a magnetic long range ordered state. This is manifested as the presence of singularities in the derivatives of the free energy $F = U - TS$. Depending on the order of the derivative with which a discontinuity occurs, one can classify two types: First order and continuous phase transitions. First order transitions have a discontinuity in the first derivative of F. Continuous transitions have a discontinuity in second or higher derivatives. For example, mean field results for FM and AFM magnetic systems give rise to the Curie-Weiss (CW) law given by

$$\chi = \frac{C}{T - \theta_{cw}} \,. \tag{2.6}$$

This is applicable in the linear[5] region in χ^{-1} above the ordering temperature. CW law allows an experimental measure of exchange strength through θ_{CW} and the effective moment through Curie constant C.

Another important feature of phase transitions is the onset of an order parameter which is due to broken symmetry. For example, the order parameter in ferromagnetic systems is the spontaneous magnetization M, which develops continuously[6] from zero at T_c.

On a fundamental level, a system that features a phase transition can be characterized by critical exponents. These determine the behaviour of divergent property (susceptibility, heat capacity, etc) and depend on elementary aspects of the system such as symmetry, dimensionality and range of interaction[45]. Some important relations are: γ (susceptibility), α (specific

[4]Dipole interactions can generally be ignored except in ions with large moments or at very low temperatures.

[5]Care must be taken to ensure the response is linear. If there are low lying crystal field levels CW cannot be used.

[6]A more useful classification instead of the classic Erhenfest definition above for the transition is whether or not the order parameter occurs abruptly (first order) or continuously (continuous).

heat), μ (correlation length). In dynamic measurements near the transition temperature the time it takes for the system to relax to equilibrium diverges as $\tau \propto \xi^z$ where ξ is the correlation length and z the dynamic critical exponent. This divergence is know as critical slowing down.

2.0.7 Percolation

To better understand and interpret the effects of dilution, and to follow the interplay between order and chaos on magnetic networks, one can utilize concepts in percolation theory. Originally, percolation theory was developed to model the formation of randomly branching polymer gels and was later used to describe fluid flows through porous media. The essence of percolation is to describe the behaviour of a randomly occupied system through the onset of connected sites that form clusters. [46] For example, which is illustrated in figure 2.2, start with an empty square lattice and begin occupying sites randomly with a probability p. A cluster is formed by occupied sites residing next to one another. As the occupation probability increases, the cluster sizes grow until a critical concentration is reached. This is called the site percolation threshold p_c and is characterized by a giant cluster that spans the entire lattice. There is a geometric phase transition from a fractured to a connected network, with the development of an order parameter, that is representative of the system. In addition to sites being occupied, another type of percolation transition exists in which the bonds between sites are randomly added. This also leads to the formation of clusters and a critical bond percolation threshold.

In the context of magnetic systems, long range magnetic order can be removed by increasing the system temperature above a critical value denoted by T_c. At this temperature, the correlation between spins is diminished and the system becomes paramagnetic. In addition, another way to shift an ordered system into a disordered paramagnetic state is through the removal of magnetic ions or the exchange interaction between them. The former is termed site dilution, where a non-magnetic ion like Mg^{2+} replaces a magnetic ion. The latter is called bond dilution where the interaction between spins is removed. For example, bond percolation can be achieved by removing oxygen ions from a magnetic oxide, thus destroying the super-exchange pathway. The effect of dilution in ferromagnetic systems results in a percolation transition at a critical concentration of magnetic ions p_c. Below this threshold, the system has a paramagnetic ground state. [45] When the fraction of magnetic

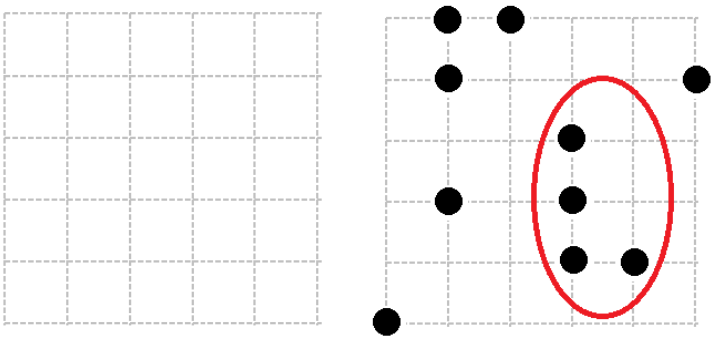

(a) (b)

Figure 2.2: Representation of site percolation on square lattice: a) Empty square lattice, b) Several lattice sites occupied with two clusters. The largest of the two clusters is highlighted in red.

ions is equal to or above p_c, there are enough magnetic sites occupied that a connected cluster spans the entire system. The size of p_c depends on several key aspects such as the dimensionality and crystal structure of the lattice. More complicated and exotic ground states can be achieved when competing interactions are coupled with dilution. The values of p_c for several important structures are given in Table 2.1.

Lattice	**site p_c**	**bond $\mathbf{p}_c$**	**q**	ref.
kagomé	0.6527	0.5243	4	[47]
triangular	0.5	0.3472	6	[47]
kagomé stack	0.3346	0.2563	6	[47]
triangular stack	0.2623	0.1859	8	[47]
spinel-type (A-site)	0.429	-	6	[8]
spinel-type (B-site)	0.39(0)	-	6	[8]
spinel-type (B-site) (4^{th} NN)	0.067	-	32	[48]
diamond	0.4495	0.3987	4	[47]
pyrochlore slab	0.50(5)	-	4	[27]

Table 2.1: Critical concentrations for site and bond percolation on several lattices with their connectivities given.

2.1 Spin Glass Behaviour

As stated above, spin glass formation hinges on the presence of both the competition between interactions (frustration) and the randomization of said interactions. The effect of these ingredients causes the system to have an enormous number of accessible states below the freezing temperature. This is true for glassy systems, structural or magnetic, which have a large amount of metastable configurations whose number grows with system size. This is can be understood as a rough phase space landscape of metastable states separated by small energy barriers. [2, 49]

Spin glasses provide unusual and distinct experimental signatures which can be broken down into local and bulk probes. Static measurements commonly done are DC magnetization, specific heat and neutron diffraction. Dynamic measurements include AC magnetization, μSR, NMR.

2.1.1 DC magnetic measurements

DC susceptibility measurements on dilute alloys, which are often termed canonical spin glasses, give a cusp in the susceptibility at the freezing temperature T_f. Detailed measurements have shown that the transition is rounded as opposed to sharp. In addition, there is an observed irreversibility in the zero field cooled (ZFC) and field cooled (FC) modes which is quite similar in

appearance to AFM ordering. Above the freezing temperature, spin glasses are paramagnetic and obey the Curie-Weiss law. [16]

Another striking behaviour of spin glasses is remnant magnetization, which measures the time evolution of the magnetic susceptibility in the frozen state. One can characterize the system by analysing the growth or decay of the magnetic moment with time after a change in applied magnetic field. Furthermore, spin glasses display a memory effect causing magnetic behaviour to depend on the cooling and magnetic field history that the sample was subjected to. The two methods used to quantify remnant behaviour and its time evolution are thermo-remnant (TRM) and isothermal remnant (IRM) magnetization. To best model the IRM and TRM data over several decades time, a stretched exponential function is used

$$M_{RM} = M_0 e^{-(\frac{t}{\tau})^{1-n}}, \tag{2.7}$$

where stretching parameter (n) and relaxation time τ characterize the glass. Previous work has shown that M_0 and n depend on temperature T ($T < T_f$) while τ is temperature independent.[50] Mean field and percolation theory restricts the values of n to fall in the range of 0 to 0.66.[51, 52] In glass theory, values of n larger than 0.66 have been reported and are believed to be due to the system being highly fragile. [53, 54] Stretched exponential functions are used in systems with a broad distribution of relaxation times. As a spin glass is cooled near its freezing temperature, there is a broadening of relaxation times which gives rise to the astronomically long time for the system to find equilibrium. [54]

2.1.2 AC magnetic measurements

AC susceptibility measurements, which yields the in phase $\chi^{'}$ and out of phase $\chi^{''}$ components of the dynamic susceptibility, allow one to probe the dynamics of a magnetic system. This is especially important in spin glasses were equilibration times diverge at T_f. This manifests as an inability of the spins to keep up with the oscillating field at the freezing temperature which gives rise to a jump in $\chi^{''}$. This effect, along with the frequency dependence on the glass freezing temperature T_f, is the hallmark feature of spin glass compounds. To make direct comparisons of this drift with frequency between

compounds one calculates which is often[7] defined as

$$\delta = \frac{\Delta T_f}{T_f \Delta \ln(f)} \,. \tag{2.8}$$

Aside from δ, the frequency dependence of the spin glass freezing temperature can be modelled using Arrhenius type, Vogel-Fulcher-Tamman law, power law, and stretched exponential. [55] The physical basis for applying these models is phenomenological and a selection of a particular one is often based on fit quality. In the Arrhenius model, which is often used in superparamagnetic systems (τ is the inverse of AC driving frequency f)[56] and is described by

$$\tau = \tau_0 e^{\frac{E_a}{k_b T_f}} \,. \tag{2.9}$$

In spin glasses, one often finds that an Arrhenius expression yields nonphysical results for the characteristic relaxation time τ_0 and activation energy E_a. [57] This deviation from Arrhenius behaviour is a characteristic of a fragile glass. A modification of the Arrhenius form yields the Vogel-Fulcher-Tamman (VFT) law which was developed in structural glass literature to describe the temperature dependence of viscosity. [58] It can be applied in systems with a broad distributions of relaxation times using

$$\tau = \tau_1 e^{\frac{E_a}{k_b (T_f - T_0)}} \,, \tag{2.10}$$

where T_0 is a measure of interaction strength between neighbouring clusters of spins, τ_1 is the characteristic[8] system time, and E_a is the activation energy. This form, although useful, creates ambiguity as T_0 is assigned in an ad-hoc manner to obtain what is believed to be physically relevant values for τ_1. [55] To remedy this issue, one can utilize a power law form reminiscent of expressions used in other critical phenomena

$$\tau = \tau_* \left(\frac{T_f - T_g}{T_g} \right)^{-zv} \tag{2.11}$$

where T_f, τ_*, T_g are the frequency dependent freezing temperature, the char-

[7]Early references to this parameter dilute alloys utilized $\log_{10}$ instead of the more recently used ln. This has led to some confusion in literature and incorrect comparisons.

[8]This has the same meaning as τ_0 in Equation 2.9 but has a different subscript to differentiate the two models.

acteristic relaxation time, and the static freezing temperature (AC driving frequency $\rightarrow$ 0) respectively. Rather than fitting all three parameters simultaneously, T_g can be determined by the peak in the DC susceptibility. Motivation for this expression stems from $\tau = \tau_* \xi^z$ where ξ is the spin correlation length, z the dynamic exponent and v is the critical exponent of the correlation length. [16]

2.1.3 Heat Capacity

Interestingly, specific heat measurements on spin glass compounds yield no singularity but rather a broad feature just above the freezing temperature. In addition, the lower temperature form of the magnetic heat capacity is linear for most spin glasses.[16] There have been exceptions of this behaviour such as magnetoplumbite $SrGa_{12-x}Cr_xO_{19}$ (SCGO(x)) whose structure was described in section 1.1. Instead of the expected linear behaviour SCGO(x) the magnetic specific heat exhibits a quadratic low temperature dependence.

Chapter 3

Methods

3.1 Sample Preparation

Solid state synthesis techniques were employed to form polycrystalline samples of $Ni_{2-x}Mg_xGeO_4$, $Co_{2-x}Mg_xGeO_4$, and $Ni_{1-x}Mg_xAl_2O_4$. High purity, dry oxides: NiO, Co_3O_4, GeO_2, MgO and Al_2O_3 (Alfa Aesar) were used as starting materials. All powders were wet milled in an agate pestle, in acetone, during each stage of synthesis to reduce particle size and create a homogeneous mixture.

The heating procedure for forming $Ni_{2-x}Mg_xGeO_4$ (x=0, 0.1, 0.2, 0.3, 0.4, 0.5, 0.10, 0.15, 0.30, 0.45, 0.60, 0.80, 1.0) was taken from Lashley *et al*[7]. Stoichiometric amounts of the starting materials were wet milled and placed in an alumina crucible with lid and fired at 1473 K for 4 hours in air. Once cooled, the mixture was wet milled and fired again at 1473 K for 4 hours. Lastly, the cooled powder was wet milled and formed into 11 mm pellets using a stainless steel pellet press. The pellets were placed in an alumina crucible and fired at 1373 K for 4 hours.

The synthesis method for $Co_{2-x}Mg_xGeO_4$ (x=0, 0.05, 0.10, 0.15, 0.30, 0.45, 0.60, 0.80, 1.0, 1.2) was adopted from Diaz *et al*[5] which uses Co_3O_4 instead of CoO. The mixed valency Co_3O_4 reduces to CoO_2 at temperatures above 800 K. Stoichimetric amounts of the starting materials were wet milled and fired at 1000 K in air for 20 hours in an alumina boat. This time was selected to ensure that Co_3O_4 is converted to CoO_2. The powder was wet milled and fired under identical conditions. Finally, the powder was wet milled and formed into 11 mm pellets using a stainless steel pellet press. The pellets were placed in an alumina crucible and fired at 1273 K for 20 hours.

The heating procedure for forming $Ni_{1-x}Mg_xAl_2O_4$ (x=0, 0.125, 0.25, 0.375, 0.5) was as follows. Stoichiometric amounts of the starting materials were wet milled and placed in an alumina crucible with lid and fired at 1473 K for 12 hours in air. Once cooled, the mixture was wet milled and fired under conditions identical to the previous step. Lastly, the powder was wet

milled and formed into 11 mm pellets using a stainless steel pellet press. The pellets were placed in an alumina crucible and fired at 1473 K for 12 hours. Recently, issues were found with site inversion of the A and B sites in related compound $MnAl_2O_4$ that drastically affected its magnetic properties. The parent was formed using a slow cooling synthesis which has been shown to reduce inversion.

3.2 X-Ray Diffraction

X-ray powder diffraction patterns on NGO were measured on an ENRAF-NONIUS diffractometer using a Cu source x ray tube. A Ni filter was used to block K_β radiation with a graphite single crystal as a collimator. Several x-ray powder diffraction patterns for CGO and NAO were measured, using a STOE-P two circle diffractometer with a Mo source, by Kevin Caslin, at the Max-Planck Institute for Solid State Research in Stuttgart, Germany.

3.3 Magnetic Measurements

DC magnetic measurements were done using a Quantum Design Magnetic Properties Measurement System (MPMS). All samples were weighed and mounted on a plastic straw with negligible magnetic contributions compared to the sample moments.

High pressure measurements were taken using a custom built pressure cell which is capable of reaching 1.2 GPa. Degassed glycerine was used as a pressure medium and high purity lead (99.999%) as a manometer. Internal cell pressure was determined by measuring the superconducting transition of the lead[59] which was placed in a teflon capsule along with the sample. The cell was mounted to the sample rod using a small copper wire. Wait times of 60 seconds were used between successive scans to allow the sample and holder temperatures to equilibrate.

AC magnetic measurements were completed on a Quatum Design Physical Properties Measurement System (PPMS) using the AC susceptibility option. All samples were weighed and mounted on a plastic straw with negligible magnetic contributions compared to the sample moments. The sample was centered inside the pickup and drive coil assembly. The real and imaginary components of the magnetic moment were measured at several frequencies in

the range of 500 Hz to 10 kHz. The drive moment had an amplitude in the range of 1 to 3 Oe. Care was taken to reduce the measurement time and/or drive moment to reduce the effects of Joule heating at temperatures below 5 Kelvin. No DC bias field was used.

3.4 Specific Heat

The heat capacity was determined using a Quantum Design Physical Properties Measurement System (PPMS) with a specific heat option. This consisted of a puck that contains a sample platform suspended by eight small wires. The system uses a thermal relaxation technique to determine the heat capacity of the platform and all materials thermally coupled to it. Apiezon N grease was used to mount the sample to the platform. Background data measurements on the sample holder and N grease were completed to enable this contribution to be subtracted from the grease-sample-platform. Care was taken in the range of 200 to 300 Kelvin as the grease melts in this temperature range which has a substantial contribution. To remedy this, Quantum Design recommends to take data points every 5 K, which was done. For all samples, measurements were taken during cooling. Please see the Appendix A for a sample plot of the Addenda and characteristic heating time constant τ_1 for $GeNi_2O_4$.

Chapter 4

Frustrated $GeNi_{2-x}Mg_xO_4$

4.1 Results

4.1.1 X-Ray Diffraction

Powder diffraction data was analysed using the Fullprof software package [60] to determine phase formation and lattice constants for all samples. The refinement results are illustrated in Figures 4.1 and 4.2. No impurity phase or starting material Bragg peaks were observed. A compilation of all refinement data is found in table 4.1. There is an observed expansion of lattice parameter, illustrated in the inset in Figure 4.1, with increasing dilution that does not appear to be linear in nature as expected from Vergard's Law. [61] An expansion of lattice parameter resulting from the substitution of Mg with Ni is expected as the crystal radii of Mg and Ni are 0.71 Å and 0.63 Å respectively. [62] However, the non-linear response observed here may stem from differences in the atomic radii of Mg^{2+} and Ni^{2+} in an octahedral environment. Denton *et al* [61] highlighted the importance of relative ion sizes regarding lattice constant and predicted non-linear response in systems with $\alpha = 0.88$, where α is the ratio of ionic radii ($\alpha = 0.89$ for Mg^{2+}, Ni^{2+}). At dilution levels of approximately 55%, $GeNi_{2-x}Mg_xO_4$ crystallizes in both olivine and spinel forms, with full Mg substitution in the spinel structure only possible when high pressure synthesis techniques are used. [34]

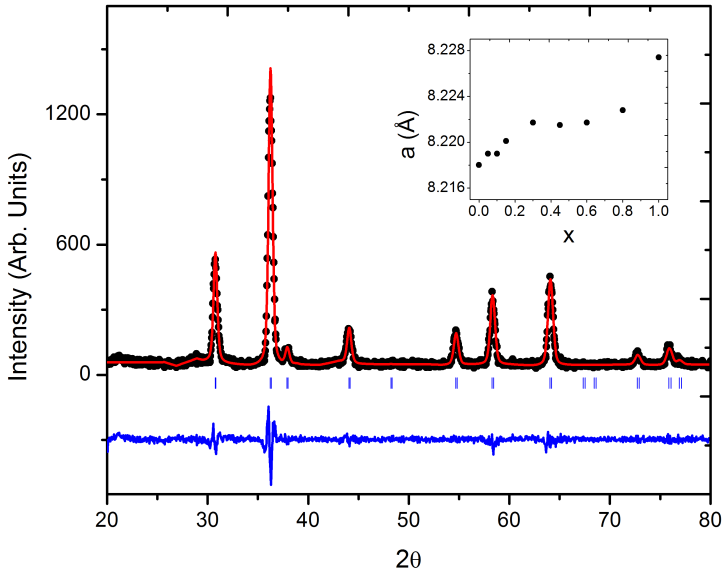

Figure 4.1: Powder diffraction and refinement results for $GeNi_2O_4$. The inset graph shows the evolution of cubic lattice parameter **a** with dilution x.

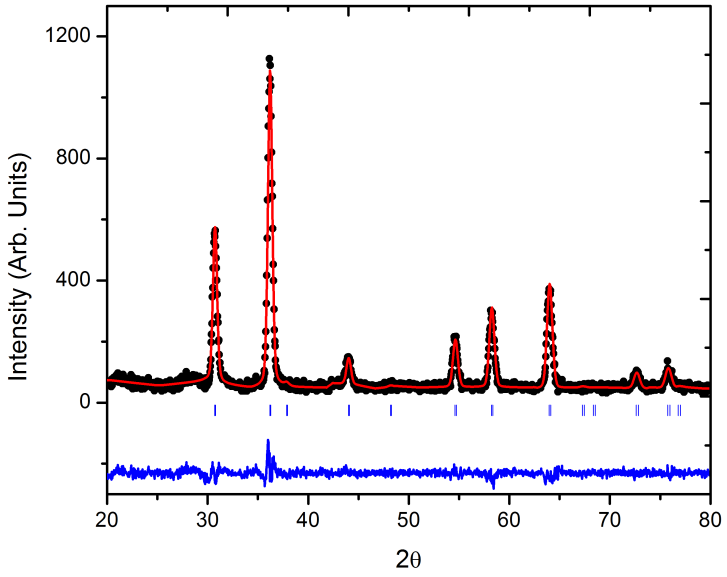

Figure 4.2: Powder diffraction and refinement results for $GeNi_{1.0}Mg_{1.0}O_4$.

Table 4.1: Summary of data on samples. Superscripts n, +, and f indicate Néel ordering, indeterminate, and spin glass freezing respectively.

Dilution (%)	$T_{n,f}$ (K)	$\theta_{CW}(K)$	a (Å)	χ^2
0	^{n}11.41, ^{n}12.01	15.0 ± 0.5	$8.218 \pm 6 \times 10^{-3}$	1.63
2.5	^{n}10.89	14.8 ± 0.2	$8.2190 \pm 3 \times 10^{-4}$	1.36
5.0	$^+$9.0	15.1 ± 0.2	$8.2189 \pm 3 \times 10^{-4}$	1.6
7.5	$^+$7.76	13.5 ± 0.3	$8.2201 \pm 3 \times 10^{-4}$	1.69
15	^{f}7.41	9.4 ± 0.3	$8.2217 \pm 3 \times 10^{-4}$	1.37
22.5	^{f}7.03	9.2 ± 0.3	$8.2215 \pm 3 \times 10^{-4}$	1.3
30	^{f}6.75	9.1 ± 0.2	$8.2217 \pm 3 \times 10^{-4}$	1.36
40	^{f}6.14	7,52 ± 0.09	$8.2228 \pm 3 \times 10^{-4}$	1.4
50	^{f}5.35	6.40 ± 0.07	$8.2274 \pm 2 \times 10^{-4}$	1.27

4.1.2 DC Susceptibility

DC susceptibility data have been reported in literature for Ni_2GeO_4 but inconsistencies exist between authors. For example, ordering temperatures T_{N1} and T_{N2} of 11.4K and 12.0K are agreed upon; however, various Curie-Weiss (CW) temperature Θ_{CW} values such as -15 K [5], -8.7 K [7], -4.4 K [3] are reported. The measurements reported here for Ni_2GeO_4 successfully reproduced the CW results obtained by Diaz *et al* through the addition of a diamagnetic term $\chi_{dia} = -7.20 \times 10^{-5}$ emu/mol_{NGO} and a temperature independent term $\chi_{ind} = 7.42 \times 10^{-4}$ emu/mol_{NGO}. This value is reasonable for Ni^{2+} in an octahedral crystal field environment with a splitting of 8,000 cm^{-1}. [63] This is given by

$$\chi_{ind} \propto \frac{4}{\Delta} \tag{4.1}$$

where Δ is the wavenumber splitting to the first excited state which is large enough to not be thermally populated. These contributions were scaled appropriately for the analysis of each diluted sample.

Results from DC magnetic data analysis are given in table 4.1. One can identify two regions ($0.15 \leq x \leq 0.6$ and $0.60 \leq x \leq 1.0$) of linear behaviour in θ_{CW} with respect to dilution. Extrapolating a linear fit line to full dilution yields $\theta_{CW} = 0$ within associated error. A similar kink in $\theta_{CW}(p)$ has been observed in other diluted frustrated systems, such as $SrGa_{12-x}Cr_xO_{19}$. [31]

In spin glasses, when the system is cooled below the freezing temperature, the magnetic moments associated with ions with unpaired electrons freeze in a metastable state. [2] The lack of a well defined ground state gives rise to this instability. This can be probed using thermoremenant magnetization (M_{TRM}) which measures the decay of the magnetic susceptibility with time. Our cooling and field routine consisted of applying a 2,000 Oe field at 300 K. The system was cooled to 2K over 12,000 seconds. The field was then turned off following a wait time of 600 seconds. Once the applied field was removed, the magnetization is measured consecutively for 10,000 seconds.

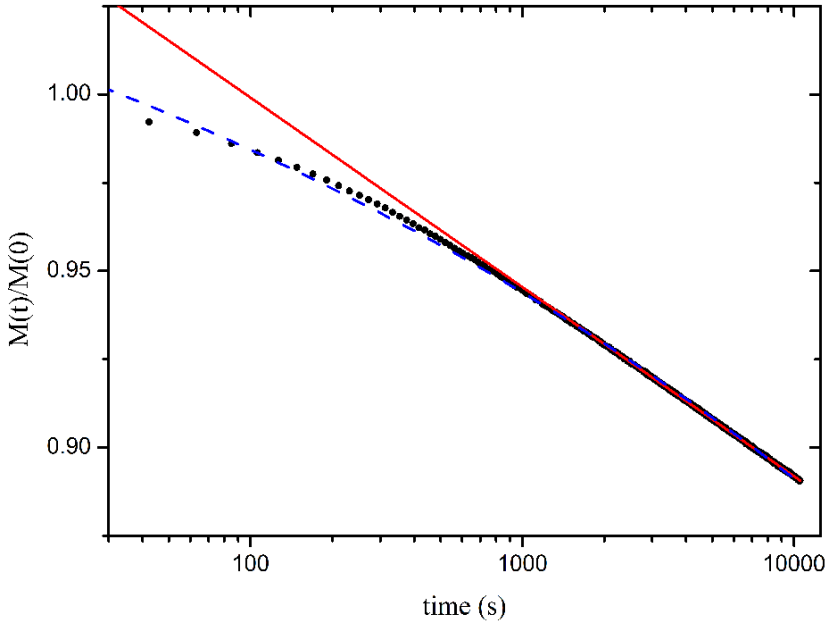

Figure 4.3: M_{TRM} data from $GeNi_{1.0}Mg_{1.0}O_4$. The dashed line is the resulting fit using a stretched exponential. The solid line is a linear fit which is constrained to the linear portion of the data.

The decay of the resulting moment is illustrated in Figure 4.3 and is normalized to the initial value measured at $t = 0$. A constrained linear function and a stretched exponential function,

$$M_{\mathrm{TRM}} = M_0 e^{-(\frac{t}{\tau})^{1-n}} \tag{4.2}$$

with stretching parameter $1 - n$, was used to fit M_{TRM}. The stretched exponential, shown in equation 4.2, generates a much better reproduction of the

experimental data. In structural glass theory it is known as the Kohlrausch-Williams-Watts (KWW) law and it is used to describe relaxation in physical properties of super-cooled liquids. [64, 65] In the context of magnetic glasses, this expression has been applied above and below T_g [66] with n exhibiting a temperature dependence near T_g. [50] For NGO spin glasses, the values obtained for n are equal within associated error and have a mean of $n = 0.861$ with a standard deviation of 0.002. This falls outside the boundaries predicted using mean field percolation in glassy systems. [52] Departure from this mean field prediction is not unusual, as data from structural glass formers have yielded similar results and are a characteristic feature of fragile glasses. Physically, n is a measure of broadness in the relaxation spectrum of the system which results in a deviation from Debye-Arrhenius behavior. [67, 56]

4.1.3 Heat Capacity

The specific heat was measured for diluted samples (x=0 to 0.30) in the temperature range of 2 to 300 K. The total heat capacity can be decomposed into the sum of lattice, magnetic and electronic contributions. In NGO, the electronic contribution is negligible and can be ignored. To obtain the lattice contribution a common approach is the use the low temperature limit ($T < \theta_D/50$) of the Debye model. [68] In NGO, particularly the diluted samples, the ordering phenomena requires the addition of magnetic correlations just above T_n and both gapped and ungapped spin wave contributions to the heat capacity. [7] An alternative method [69] based on Padé approximants, which was employed here, allows one to fit convenient regions of the specific heat data to obtain the lattice contribution. The total heat capacity can be expressed as:

$$C_p = C_{mag} + A * C_{padé} + B * C_{E1} + C * C_{E2} \tag{4.3}$$

where the last three terms model the lattice contribution and the sum of A,B and C is 7.[1] The Padé approximant is designed to reproduce the Debye function through all temperature ranges. It therefore only models acoustic phonons and fails to accurately reproduce the contributions from optical modes. [68] To remedy this two Einstein terms, C_{E1} and C_{E2}, have been added which take the form of

[1] Due to 7 atoms in each unit of GeN_2O_4.

$$C_E = 3R\left(\frac{T_E}{T}\right)^2 \frac{e^{T_E/T}}{(e^{T_E/T}-1)^2}, \tag{4.4}$$

T_E is the corresponding Einstein temperature and R is the gas constant.

Figure 4.4 illustrates experimental data for $Ni_{1.99}Mg_{0.01}GeO_4$ and the resulting fit using the last three terms of equation 4.3. The temperature range for the fit is 100 K to 300 K which was selected to be sufficiently far away from the magnetic transitions such that they have a negligible contribution to the specific heat.

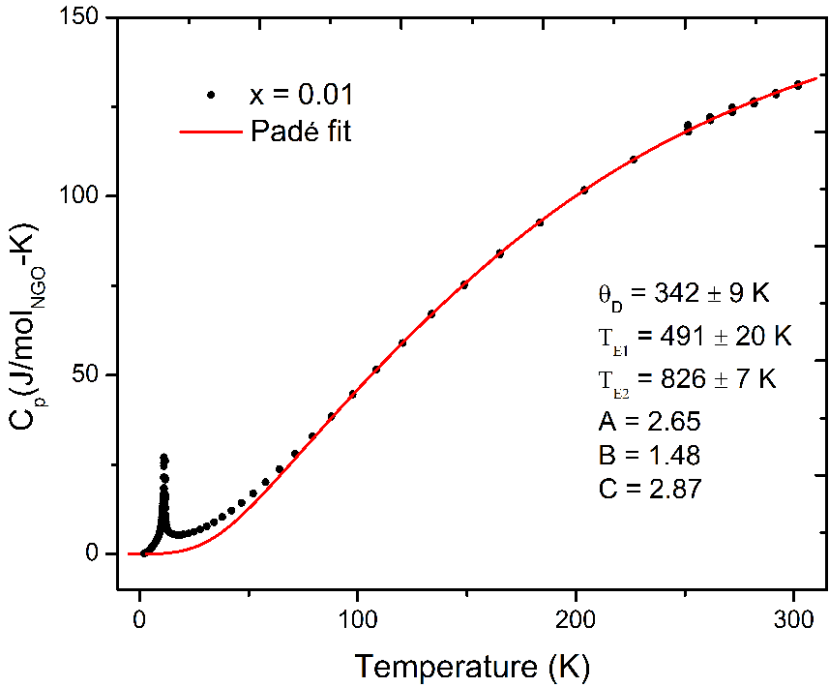

Figure 4.4: Specific heat of $Ni_{1.99}Mg_{0.01}GeO_4$. The data is fitted from 120 K to 300 K to the last three terms of equation 4.3 with the fit line extrapolated to 0 K.

The Debye temperature obtained is Θ_D 342 ± 9 K, which is smaller than the value of 386 K obtained by Lashley. [7] Possible reasons for this difference could be the usage of the low temperature Debye form at temperatures as high as 75K. Due to the approximations made in the Debye model, the value of Θ_D varies with temperature. This variation is minimized [68] in

the temperature regions $T < \theta_D/50$ (7.72 K) and $T > \theta_D/2$ (193 K) if the $\theta_D = 386$ K value is assumed.

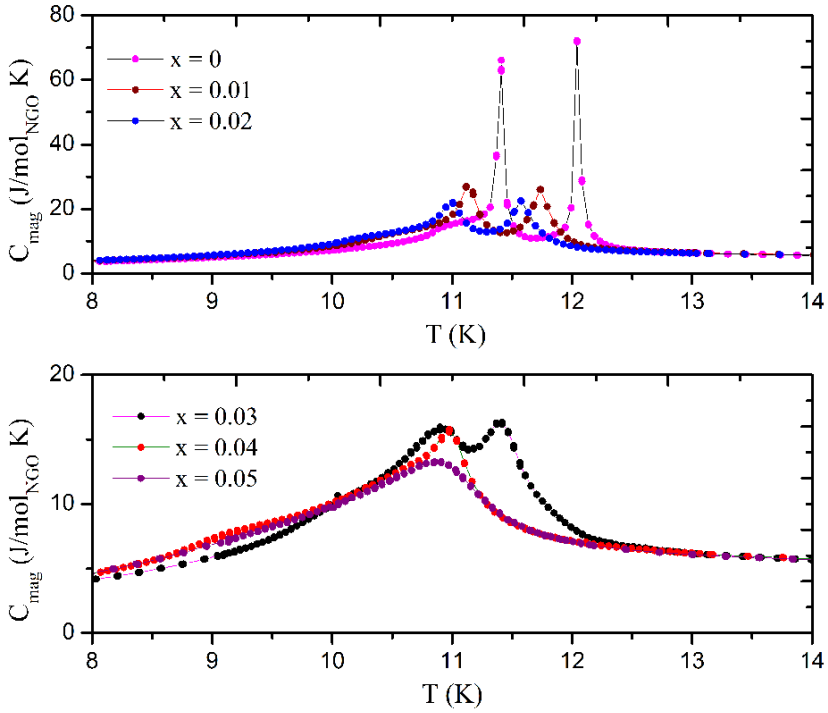

Figure 4.5: Plot of the magnetic contribution to specific heat for several diluted samples of $GeNi_{2-x}Mg_xO_4$.

With the lattice contribution determined, the magnetic contribution can easily be determined which is shown in Figure 4.5. There is a reduction and broadening of the peaks in the specific heat with increasing dilution which is evidence of a shift from long to short range ordering. We observe the disappearance of T_{N2} at 2.0% ($x = 0.04$) dilution while T_{N1} persists in a visible but broadened form. These results indicate the destruction of long range order upon random site dilution occurs first in the triangular planes, followed by the kagomé planes. This is interesting since one would expect dilution to affect kagomé ordering to a greater degree as there are three times the number of spins on the kagomé planes. A Mg^{2+} ion is three times more likely to sit on a kagomé plane if the dilution is random. One may interpret these results as an indication that the stability of LRO in the triangular planes depends strongly on the kagomé layers that separate them.

4.1.4 AC Susceptibility

With the destruction of long range order, the dynamic susceptibility becomes an important probe for determining the nature of the low temperature state. AC susceptibility measurements were completed on samples in the dilution range of $x = 0.15$ to 1.00 at 500, 1000, 5000 and 7000 Hz. Data for these dilution values taken at 7000 Hz is shown in Figure 4.6. Onset of canonical spin glass behaviour can be seen in dilution levels at and above 15% ($x = 0.30$). In spin glasses the freezing temperature T_f can be defined as the cusp in the real part of the AC susceptibility $\chi^{'}$ and a spike in the imaginary part of the susceptibility $\chi^{''}$. This behaviour is due to the inability of spins to keep up with the oscillating applied field, due to diverging relaxation times, which causes a non-zero out of phase component $\chi^{''}$. [16]

There is a decrease in freezing temperature T_f with dilution which follows a nearly linear response in the spin glass regime ($0.15<x<1.00$). Extrapolation of the data yields a non physical result of approximately x=3 for 0 K freezing temperature.

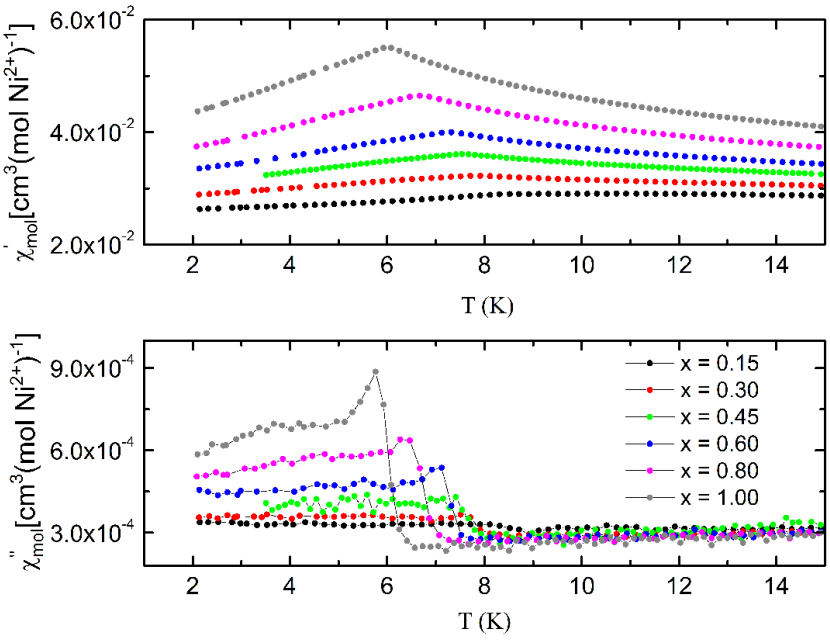

Figure 4.6: Plot of the AC susceptibility of diluted $GeNi_{2-x}Mg_xO_4$ samples taken at 7,000 Hz.The cusp in the real part and jump in the imaginary part of the dynamic susceptibility are evidence of spin glass freezing.

Table 4.2: Summary of data on $GeNi_{2-x}Mg_xO_4$ samples.

Dilution (%)	zv	$\tau_*(10^{-15}s)$	$E_a(eV)$	$T_0(K)$
15	7.8 ± 1.0	3.2 ± 0.3	2.8 ± 0.2	6.44 ± 0.09
22.5	7.92 ± 0.6	19 ± 3	2.7 ± 0.2	6.03 ± 0.08
30	9.6 ± 0.6	0.50± 0.02	1.88± 0.06	6.34 ± 0.03
40	8.7 ± 0.3	17 ± 0.9	2.6 ± 0.1	5.28 ± 0.04
50	10.7 ± 0.3	2.8 ± 0.07	2.8 ± 0.1	4.56 ± 0.03

An observed frequency dependence on T_f exists and is a characteristic feature of spin glasses and systems with broad distributions of energy levels. [51, 16] One way to compare this dependence between different systems is to calculate σ, using Equation 2.8, which is a measure of the drift of T_f with respect to driving frequency. The value of sigma can be used to determine the level of interaction between the glassy constituents (clusters or individual spins) of the spin glass. For weakly interacting systems such as $La_{0.994}Gd_{0.006}Al_2$ [70] δ takes a value of 0.056. Conversely for systems with stronger interactions such as canonical spin glasses δ has an approximate range of 0.002. [57] In $Ni_{2-x}Mg_xGeO_4$, δ takes values: 0.0061, 0.0074, 0.0065, 0.0084, 0.0091 for dilution levels of $x = 0.30$, 0.45, 0.60, 0.80, 1.00 respectively.

The frequency dependence of the spin glass freezing temperature was also modelled using Arrhenius type, Vogel-Fulcher-Tamman law, and power law, which were discussed in Section 2.1.2. Upon fitting the experimental data to the Arrhenius model, non-physical values the characteristic relaxation time τ_0 and activation energy E_a where obtained. This has been known to occur in systems with broad distributions of relaxation times. [57]

To make progress in the analysis, both the VFT and power law models were used to fit the experimental data which is illustrated in Figure 4.7, with values for the fitted parameters found in Table 4.2. Both models fit the experimental data well. However, the VFT model creates ambiguity through the ad-hoc assignment of T_0 to obtain what is believed to be physically relevant values for τ_1. [55] The power law model does not suffer from this drawback as it contains only two fit parameters, as discussed in Section 2.1.2. This leaves only the product of the critical exponents $z\nu$ and characteristic time τ_*.

The characteristic relaxation time of the spin glass system τ_* ranges from

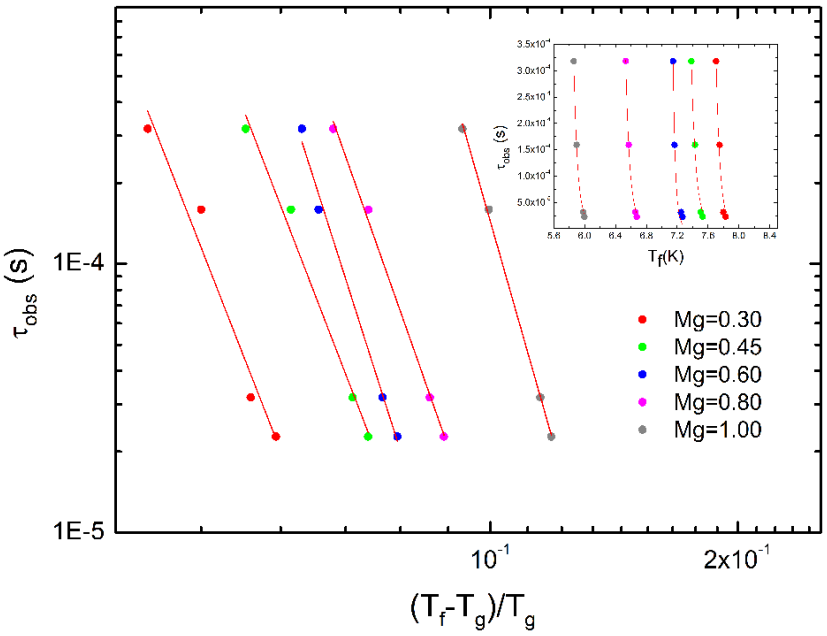

Figure 4.7: Plot of AC freezing temperature data fitted to equation 2.11. Inset graph illustrates the same data fitted using the acting spins.VFT equation.

10^{-14} to 10^{-16} seconds which indicative of canonical spin glass behaviour. Contrast this with the cluster glass systems like $La_{1.85}Sr_{0.15}Cu_{1-y}Ni_yO_4$, $Li_xNi_{2-x}O_2$ and $CaBaFe_{4-x}Li_xO_7$ which have τ_* values of $10^{-9.5}$, 7.5×10^{-11} and 4.9×10^{-12} seconds respectively. The values of the critical exponent zv obtained vary from 7.8 to 10.7 and fall within the range 5 to 11 found for several spin glass compounds. [55]

4.1.5 High Pressure Effects

Lattice distortion is an important means by which frustration can be relieved. This is evident particularly in the related spinel $GeCo_2O_4$ which undergoes a simultaneous cubic to tetragonal distortion and antiferromagnetic transition where c/a $\approx$ 1.0014. [71] To the authors' knowledge, there have been no observations of a structural transition in NGO using neutron or synchrotron x-ray probes. [3] The relation between lattice constant and the corresponding magnetic properties of NGO can be further tested using high precision

thermal expansion measurements. The results are illustrated in Figure 4.8 where the reference length L_0 is $L(T = 20)$. The two AFM transitions are clearly indicated by a steep decrease in strain $\Delta L \backslash L_0$ signalling lattice constant shrinkage. This decrease is affected by applied magnetic field and is most noticeable at the kagomé ordering temperature T_{N1}. Specifically, the change in strain at T_{N1} is -6.899×10^{-6}, -4.943×10^{-6}, 1.082×10^{-6} for fields of 0, 1.5, and 6.0 T respectively. A similar field induced transition in the nature of TE response has been observed in $EuTiO_3$ [72] where a cross over between contraction and expansion occurred at 0.675 T with destruction of long range order at 1 T. Conversely, NGO is very robust against applied fields with a spin flop transitions at H_1=30 T and H_2=37 T at 4K. [4]

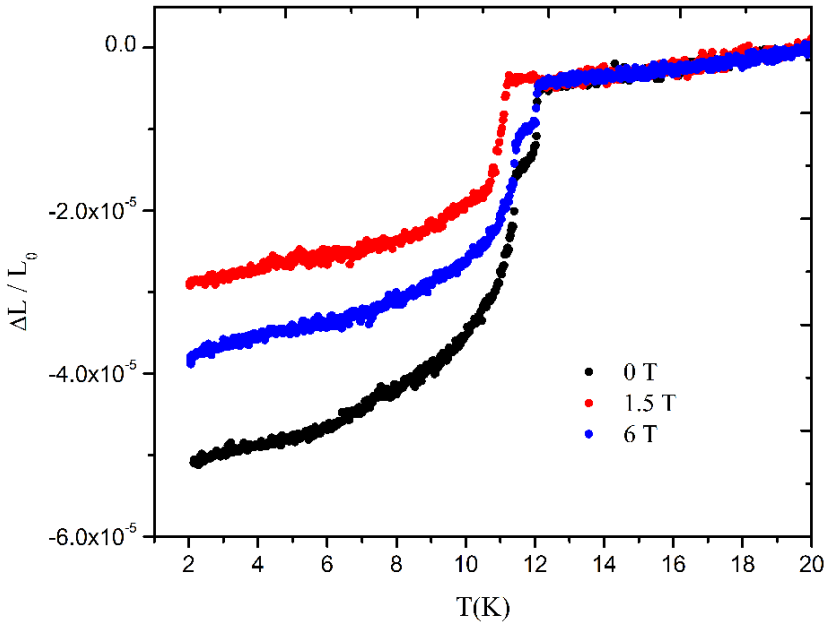

Figure 4.8: Strain $\Delta L \backslash L_0$, taken at various applied fields, where L_0 is the reference length at 20 K. The onset of magnetic transitions are denoted by a rapid change in strain.

This indeed confirms a spin-lattice coupling occurs in NGO. To further test the effects of perturbations on Ni_2GeO_4 quasi-hydrostatic high pressure susceptibility measurements were taken on a polycrystalline sample in the range 0 to 1.2 GPa. To estimate the effect of applied pressure on the lattice it is noted [73] that several related spinel compounds have bulk moduli K

that lie in between 170 to 210 GPa. Using an estimated value of 200 GPa the strain can be approximated using $K = -V\Delta P \backslash \Delta V$ where $\Delta V \approx 3L^2\Delta L$ the maximum strain is 1E-3.

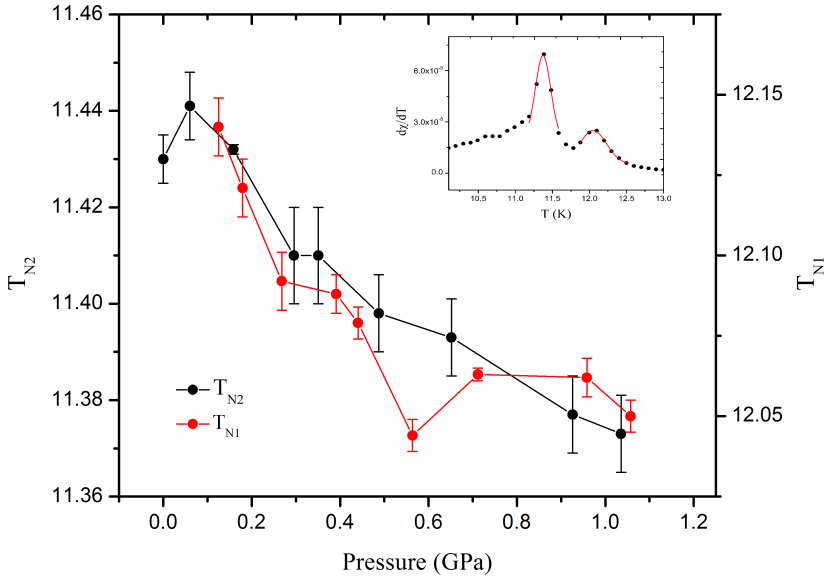

Figure 4.9: Antiferromagnetic transitions T_{N1} (kagomé) and T_{N2} (triangular) in $GeNi_2O_4$ at various applied pressures. The inset graph depicts fits to peaks in $d\chi \backslash dT$.

Figure 4.9 illustrates the effect of applied quasi-hydrostatic pressure on the two AFM transitions of polycrystalline NGO. These were determined by fitting Gaussian peak functions to maxima in $d\chi \backslash dT$ which is shown in the inset. There is a small decrease of similar magnitude in the ordering temperatures T_{N1} and T_{N2}. The result that both transitions have nearly identical responses is somewhat striking for several reasons. First, the kagomé and triangular planes order independently, yield vastly different lattice effects under applied fields. Furthermore, the exchange connectivity for each plane type is different with the kagomé planes having more nn that reside within themselves. These results depict a magnetically robust system that can withstand lattice changes of varying degree but still maintain the necessary balance in exchange interactions that yield two AFM transitions.

4.2 Discussion

Combining the results from specific heat, AC and DC susceptibility measurements, one can construct a phase diagram which is shown in Figure 4.10. There are 3 distinct magnetic phases separated by an indeterminate region defined by two dilution values of $x = 0.10$ and $x = 0.15$. In these samples the features indicating LRO such as: sharp peak in the magnetic specific heat, and point of inflection in χ_{DC} (peak in $d\chi_{DC}/dT$) are not well defined. Furthermore, there is no indication of a spin glass transition in Figure 4.6.

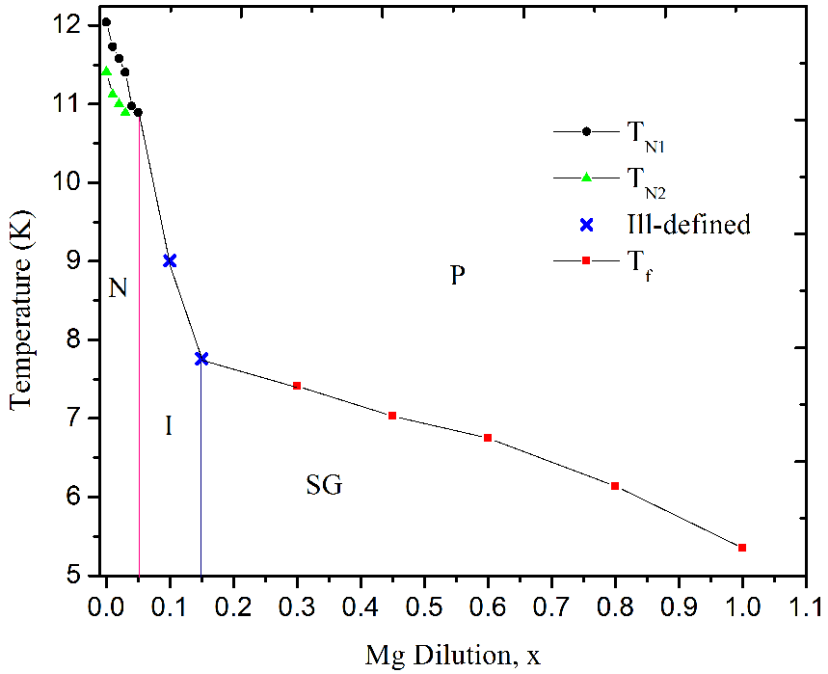

Figure 4.10: Experimental phase diagram of $GeNi_{2-x}Mg_xO_4$. There are 4 distinct regions: N - Neel ordered, I - ill defined, SG - spin glass, and P - paramagnetic.

4.2.1 Low Dilution (x < 0.10)

The effects of B site magnetic dilution clearly have a dramatic effect on the two long range ordered low temperature states. The magnitude of this effect is different for the different planar types that make up the B site sub-lattice.

Figure 4.10 illustrates that long range order persists in the kagomé and triangular planes up to dilution values up to x=0.05 and x=0.03 respectively. In this region, the Néel temperatures associated with T_{N1} and T_{N2} evolve linearly and can be extracted to yield the critical dilution levels. This was achieved by extrapolating a linear fit of the linear regions found in Figure 4.10. Using this methond, critical dilution levels of $x_{d1} = 0.53 \pm 0.07$ and $x_{d2} = 0.70 \pm 0.1$ were obtained for the kagomé and triangular planes respectively. Critical percolation thresholds were found by taking $(2-x_d)/2$ (where x_d is the critical dilution value described above). From this, the percolation thresholds were estimated as $p_{c1} = 0.74 \pm 0.04$ for the kagomé planes and $p_{c2} = 0.65 \pm 0.05$ for the triangular planes. The expected 2d values for these planes with NN interactions are 0.652 (kagomé) and 0.5 (triangular). [47] This is an unusual result, since one would expect the experimental values of p_c to be smaller than the 2D values. NGO is the antithesis of a 2D system with large interplanar coupling which is believed to give rise to NGO's unique ground state. Increases in dimensionality should reduce p_c as the lattice becomes more connected. For example, the percolation threshold for stacked kagomé and triangular lattices have values 0.3345 and 0.2623 [47] respectively, much lower than 2D analogues. Similarly if interactions extend beyond nearest neighbours, the ordered state becomes very robust towards site removal. [48]

However, seemingly artificial levels for critical concentration are not unheard of. In the kagomé staircase $(Co_{1-x}Mg_x)_3V_2O_8$, it was found to have an x_c=0.74 instead of 0.65 for the Neél ordered state. This difference was determined to stem from the buckled nature of the kagomé staircase structure which quenches exchange interactions from the spine sites thereby increasing p_c from the expected 0.65 to 0.74. [74] In NGO, there is no evidence of major structural distortion [3], such as buckling, that would result in the loss of interactions. Furthermore, NGO is a 3D system with large spin connectivity due to its vast exchange network of up to J_4.

One possibility for this high sensitivity to dilution is the effect of coupling between the spins that reside on different plane types. That is, due to the distinct ordering of the kagomé and triangular planes, below T_{N2} one can think of the B site lattice as two, three dimensional interconnected networks: stacked triangular and stacked kagomé. These networks have connections to themselves and to each other. Factoring up to J_4 with 42 total neighbours, a single spin in the triangular network contains 12 links to other triangular sites and 30 links to the kagomé network. Conversely, the kagomé system is

much more self connected with only 10 links to the triangular network and 30 to other kagomé sites. Recent research [75] has shown that coupled networks, network of networks (NON), are more vulnerable to what is often called 'attack' which in this context is site dilution. This vulnerability is manifested as an increased percolation threshold [76] and has been observed in several different network types: Erdos-Renyi, regular random and lattice [77]. Furthermore, with increased internetwork coupling, the larger p_c becomes. This is in stark contrast to single networks where increased connectivity decreases p_c. Physically this can be understood as a diluted site on either kagomé or triangular layers affecting both its own layer type as well as the other complementary layer. This perturbation may cascade locally through both networks amplifying its effect. The net result would be a larger value of p_c due to the fragility of the entire system that stems from this cascade effect.

4.2.2 Spin Glass ($0.30 \leq x \leq 1.0$)

A broad specific heat anomaly and a jump in the imaginary component of the AC susceptibility results indicate a single spin glass transition that begins at x=0.30 (15% dilution). Somewhat surprisingly, glassiness does not form on each plane type which would give rise to two distinct freezing transitions: one for kagomé and one for triangular spins. Instead there is a single spin glass transition. It is unclear if the glass state emerges across the entire B site sub-lattice, or only on the kagomé sites while the triangular planes behave in paramagnetic fashion. Specific heat results suggest the latter case due to the apparent destruction of the T_{N2} transition in Figure 4.5, rather than the broadening and merger of both peaks. If the glass state is only composed of kagomé sites, one can compare the above results with structurally similar systems that undergo spin glass transitions.

One such system, deuteronium jarosite $(D_3O)Fe_3(SO_4)_2(OD)_6$, consists of Fe^{3+} ions (S=5/2) in stacked kagomé planes which undergoes a spin glass transition at 13.8 K. [78, 79] Specific heat results indicate an anomalous low temperature T^2 behaviour instead of the linear relationship expected for canonical spin glasses. Similar behaviour has been found in SCGO(x) spin glasses. [32] In both cases it is believed that the T^2 dependence stems from the strong 2D character of the magnetic network. [33] In the spin glass $GeNi_{1.7}Mg_{0.3}O_4$ there is also a low temperature T^2 dependence of the magnetic heat capacity, illustrated in Figure 4.11, which could indicate a similar 2D character. Furthermore, the other parameters determined to characterize

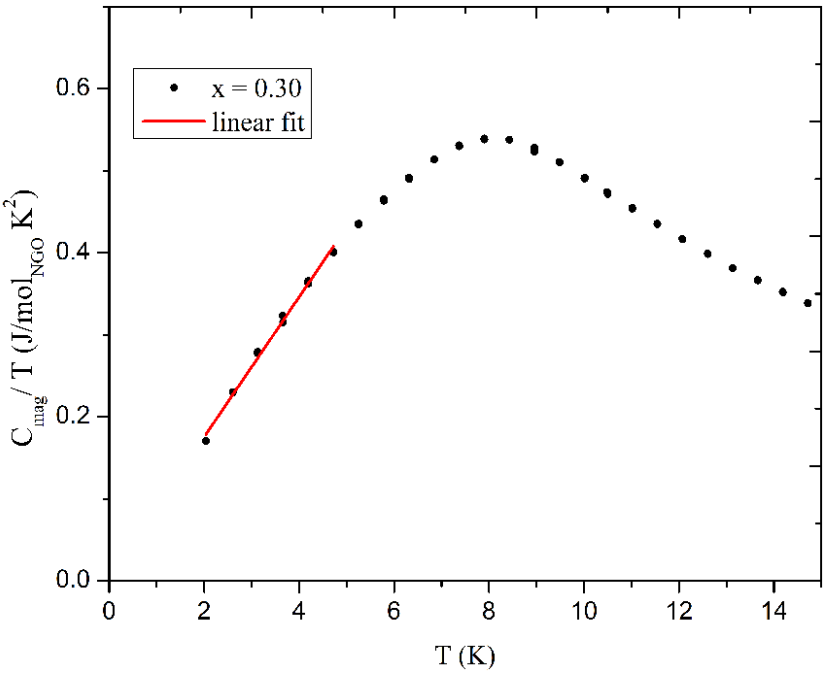

Figure 4.11: Magnetic component of C_p/T for the spin glass $GeNi_{1.7}Mg_{0.3}O_4$. The red linear fit line indicates a T^2 dependence of the magnetic specific heat at low temperature.

the glassy nature of diluted NGO compare favourably to deuterium jarosite. The values of σ determined from equation 2.8 range from 0.006 to 0.009 compared to a value of 0.010 for deuterium jarosite. [78] The numbers obtained fall closely within the values obtained for canonical spin glasses such as CuMn (σ=0.002)[80], and AuMn (σ=0.0020)[81]. [2]

4.3 Conclusion

In this chapter, the effects of magnetic dilution and spin-lattice coupling on spinel type $GeNi_2O_4$ are reported. This was undertaken to probe the nature of the long range ordered state of NGO which is formed by two closely spaced magnetic transitions, the root of which, is a complex exchange network of 32

[2]Some variations regarding the σ values for AuMn and CuMn exist, due to the original authors usage of $\log_{10}$ instead of ln in equation 2.8.

relevant neighbours. Thermal expansion measurements reveal a field dependent lattice contraction at both T_{N1} and T_{N2}. At an applied magnetic field of 6 T, there is a positive change in strain indicating a field induced cross over from lattice contraction to expansion. The phase evolution of this compound when Ni^{2+} sites are replaced with non-magnetic Mg^{2+} can be broadly classified into three regions: ordered, ill defined, and spin glass.

At dilution levels of x = 0.30 and higher, the system becomes a spin glass. AC susceptibility and TRM measurements suggest that the system is a canonical type glass. In addition there is no evidence of distinct spin glass transitions for each of the AFM transitions found in the parent compound. It appears that the triangular planes first become disordered followed by a glass transition in the kagomé planes. The magnetic specific heat in the glass state behaves as T^2 at low temperature, which is unusual for spin glass compounds, which suggests a shift from 3D long range ordered state to a 2D spin glass.

The long range ordered state of the kagomé and triangular planes are extremely susceptible to magnetic dilution. Specific heat and magnetic susceptibility measurements indicate that clear signs of magnetic ordering disappear for kagomé spins at approximately 2.5% Mg^{2+} substitution. Likewise, the ordered state for triangular spins appear even more delicate with a lack of distinct ordering at 1.5$ dilution. Through linear fits the percolation thresholds for the kagomé and triangular planar networks were found to be p_{c1}=0.74 $\pm$ 0.04 and p_{c2}=0.65 $\pm$ 0.05 respectively. These values are much larger than percolation values for stacked kagomé (p_c= 0.3346) and triangular planes (p_c= 0.2623). This perplexing result may be explained by treating the triangular and kagomé spins as a network of networks. NONs have been shown to be highly unstable to site removal which is amplified by increased connectivity. Neutron diffraction experiments currently undertaken will hopefully shed light on the nature of the ill-defined phase and the anomalously large percolation threshold. If the NON interpretation is correct, to the author's knowledge, NGO would be the first reported manifestation this effect in the solid state. Further research in other magnetic systems with distinct ordered sublattices, such as $GeMn_2O_4$ and $GeFe_2O_4$ should be studied to possibly find other candidates for the NON effect.

Chapter 5

Frustrated $GeCo_{2-x}Mg_xO_4$

5.1 Results

5.1.1 X Ray Diffraction

The Rietveld refinement method was used on X ray powder diffraction data, taken from a Mo source, to determine lattice constants for $GeCo_{2-x}Mg_xO_4$. During refinement, the relative occupancies of the Co^{2+} and Mg^{2+} were varied according to the sample stoichiometry as needed. Two examples of the refinement results are shown in Figures 5.1 and 5.2. The lattice constant decreases in a near linear fashion with increasing Mg substitution which can be seen in the inset in Figure 5.1. This is to be expected as the crystal radius for Co^{2+} in octahedral coordination is 0.79 Å compared to 0.71 for Mg^{2+} in the same environment. [62] $GeCo_{2-x}Mg_xO_4$ maintains the spinel type structure up to x = 1.20. Solubility studies on this compound have indicated that beyond a 60% Mg^{2+} concentration, a structural shift from spinel type to olivine occurs. [34]

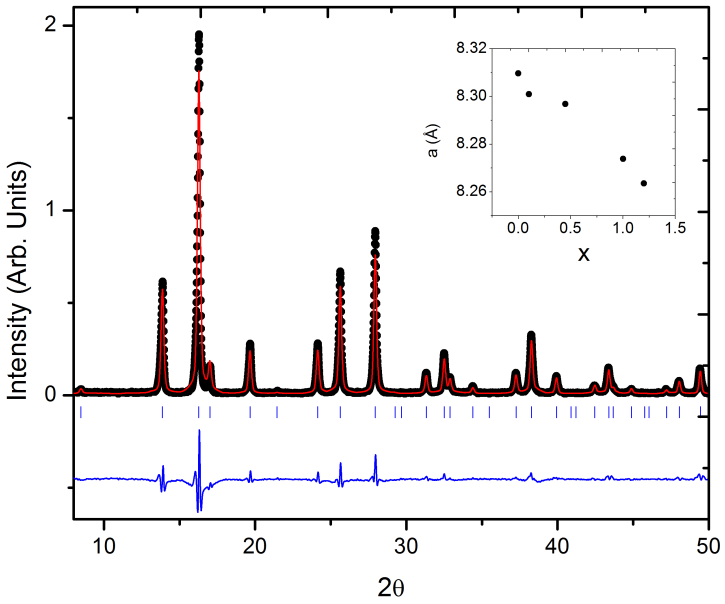

Figure 5.1: Rietveld refinement of XRD pattern for $GeCo_2O_4$. Inset is plot of lattice constant for several diluted CGO samples.

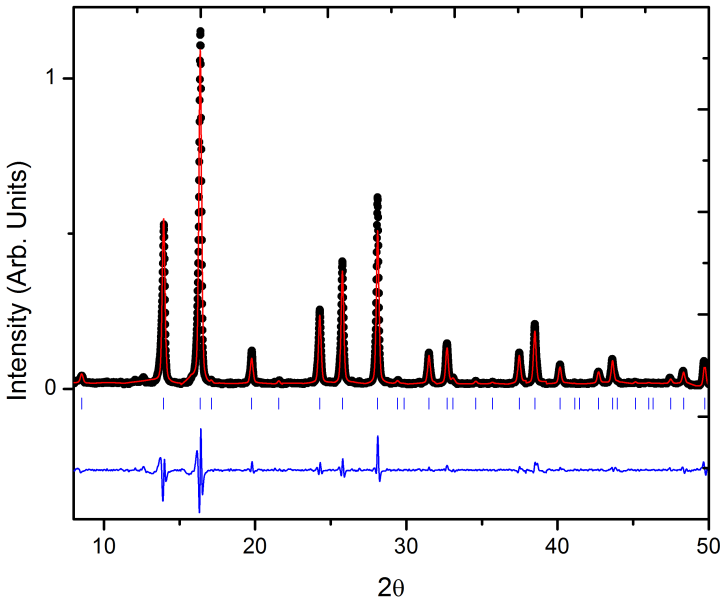

Figure 5.2: Rietveld refinement of XRD pattern for $GeCo_{0.8}Mg_{1.2}O_4$.

5.1.2 DC Magnetization

DC magnetic susceptibility measurements were completed on all samples with the results displayed in Figure 5.3. Unfortunately, it is not possible to extract information from any of these measurements using Curie-Weiss fits. This is due to a lack of linearity in χ^{-1} that stems from the thermally accessible crystal electric field levels in CGO. [7] However, despite this issue, there are several reported values for Θ_{CW}: 80.5 K [5, 82, 83], 40 K [71, 42], 47.6 K [84] whose variations may arise from different temperature regions used during the linear fit routine. In spite of this limitation, DC data can be used to begin to understand dilution effects at a qualitative level and to track the evolution of transition temperature.

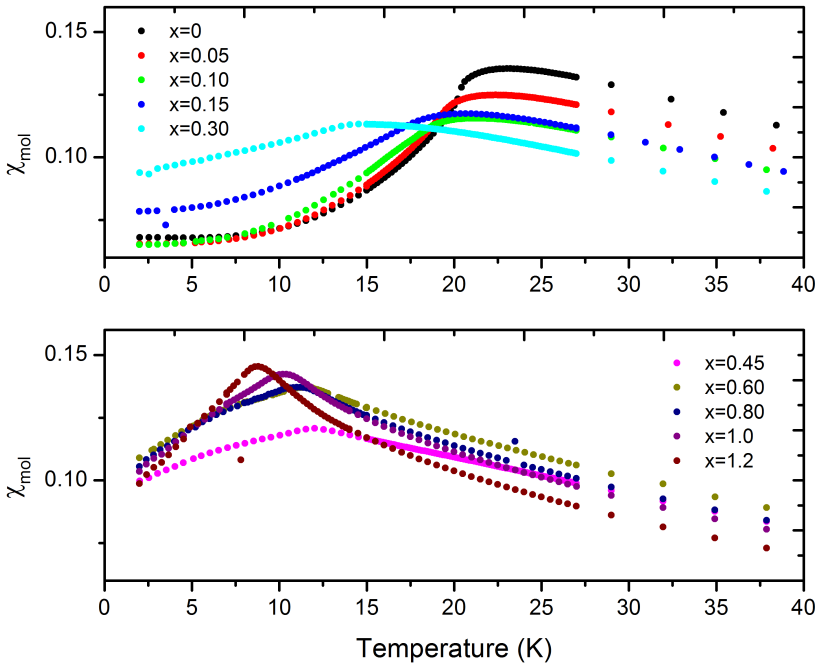

Figure 5.3: DC magnetic susceptibilities of $GeCo_{2-x}Mg_xO_4$.

From a qualitative perspective, the sharp decrease in DC susceptibility, indicative of the AFM transition, is maintained until x = 0.15 (observed as a peak in dχ/dT). Beyond this level, the response begins to look like a canonical type spin glass with a symmetric cusp forming. Another feature is the effect of dilution on the maximum value of χ. As Mg^{2+} concentration increases, there is a reduction in χ_{max} which has a minimum for x = 0.10. Above

this dilution, χ_{max} steadily increases with further dilution. This feature is observed in many insulating spin-glass materials such as SGCO [31] and $ZnCr_{2(1-x)}Ga_{2x}O_4$. [85]

The effects of aging were studied for samples with Mg^{2+} levels greater than $x \geq 0.45$ by measuring the evolution of the magnetization with respect to time (relaxation). Aging is a hallmark feature [17, 10] of spin glass materials and its characterization is often used as a method of comparison between SG materials. The measurement routine was as follows: a 2,000 Oe field was applied at 300 K. The system was then cooled to 2 Kelvin over 12,000 seconds. Once 2 K was reached, the field was removed following a wait time of 600 seconds. Immediately upon the applied magnetic field removal, the magnetization was measured consecutively for 10,000 seconds. The results are illustrated in Figure 5.4 with attempts to fit the data to a power law of the form $M(t) = M(0)t^{-\gamma}$ and a stretched exponential which is described in Section 2.7. The fit results are similar to NGO with the power law function poorly representing the full data range. The stretched exponential or (KKW form) was also used to fit M_{TRM} data for NGO in section 4.1.2. The values obtained for n are concentration independent, with an average value and standard deviation of 0.88 ± 0.03, and is very close to the value of $n = 0.861 \pm 0.002$ obtained for spin glass NGO. During the fitting routine M_0 was not constrained such that $M_{\mathrm{R}}/M_0 = 1$ at $t = 0$. This decision was made due to following: $t = 0$ is defined experimentally as the time of the first measurement following field removal, not specifically when the applied field is removed. There is a short period of time between field removal, which is the true $t = 0$, and the initial measurement. Due to the lag the measured value of $M_{\mathrm{R}}(t = 0)$ is smaller than the true value causing $M_t/M_0 > 1$ which is reflected in the fit results.

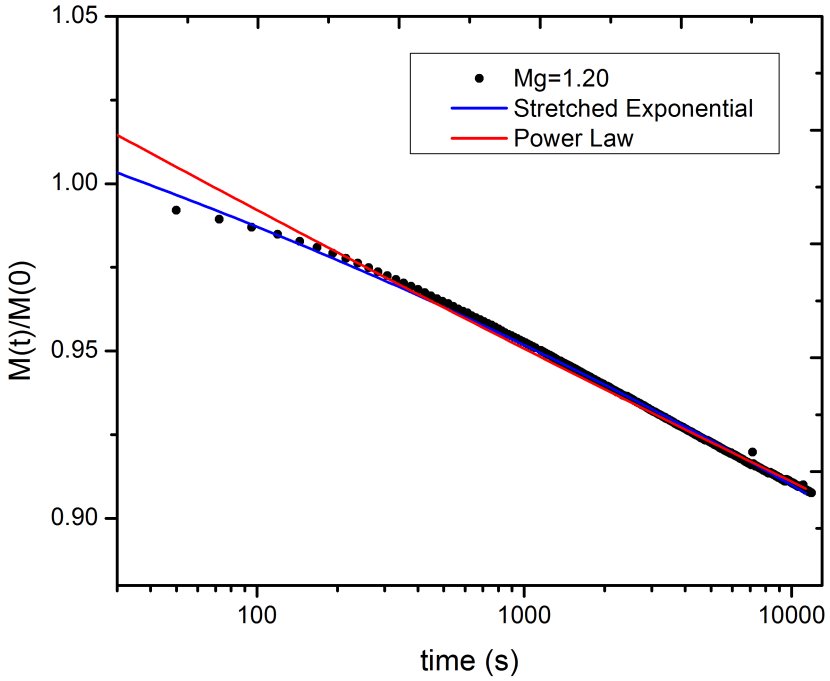

Figure 5.4: Magnetic relaxation of $GeCo_{0.8}Mg_{1.2}O_4$ with fits to a stretched exponential and a power law.

5.1.3 Specific Heat

The heat capacity of a substance not only aids in characterizing phase transitions, it is an excellent probe to gain information regarding the distribution of energy levels within a compound. This feature makes the analysis of specific heat data for $GeCo_{2-x}Mg_xO_4$ more nuanced than NGO.[1] In CGO, there are several contributions to the specific heat that are not found in NGO. These include hyperfine and crystal electric field (CEF) Schottky effects that are described below. An expression for the total heat capacity is given by

$$C_p = C_{mag} + C_{lat} + C_{hyp} + C_{CEF}, \tag{5.1}$$

in equation 5.1 with terms representing magnetic, lattice, hyperfine, and the crystal electric field (CEF) contributions. The degenerate electronic levels of the Co^{2+} ions are split into six doublets due to crystal electric field effects

[1]The analysis has some features borrowed from Lashley *et al.* [7] and Goetsch *et al.* [69]

and spin orbit coupling. Inelastic neutron scattering experiments [7] have determined that the energies of these levels are 0 K, 180 K, 360 K, 440 K, 1760 K and 1930 K. Since these are thermally accessible, the CEF levels make the following Schottky contribution to the heat capacity [68, 7]

$$C_{CEF} = R\,\frac{\sum_{i=1}^{j} d_i(E_i/T)^2 e^{-E_i/T} \sum_{i=1}^{j} d_i(E_i/T) e^{-E_i/T}}{d_0 + \sum_{i=1}^{j} d_i(E_i/T) e^{-E_i/T}} \tag{5.2}$$

where R, d_i, and E_i are the ideal gas constant, degeneracy, and energy of the i^{th} CEF level. In CGO, all six levels are doubly degenerate, with the energies given above, and have a significant influence above 20 K with maximum at approximately 180 K (see Figure 5.5). Due to this contribution being present over a large temperature range, particularly above 100 K, one must account for it in order to obtain meaningful results for C_{lat}.

In addition to CEF levels, there exists low level hyperfine energy levels that arise from the coupling of the nuclear moment of the Co^{2+} ions and the electronic moment. This causes another Schottky effect that is present at very low temperatures due to the small size of the nuclear moment. [68] Expanding equation 5.2 in the limit of small E_i/T yields:

$$C_{\text{hyp}} = R\frac{D_I}{T^2}. \tag{5.3}$$

If more than one ion with a nuclear moment is present, C_{hyp} becomes a sum. In CGO, only ^{59}Co (100% abundance, I=7/2) contributes with vanishingly small quadrupole contribution [86], so the expression for D_I becomes [7]

$$D_I = \frac{(I+1)\mu_{nuc}^2 B_{nuc}^2}{3Ik_b^2} \tag{5.4}$$

where μ_{nuc}^2 and B_{nuc}^2 are the nuclear moment and the effective hyperfine field found at the nucleus. Low temperature heat capacity measurements yield $B_{nuc}^2 = 129$ T and $D = 1.4 \times 10^{-3}$ JK/mol_{CGO}. [7] The calculated values from these two Schottky effects are plotted with raw data on $GeCo_2O_4$ in Figure 5.5 which underscores the relative size of each contribution.

With the hyperfine and crystal electric field contributions removed, only C_{lat} and C_{mag} remain. The magnetic contribution is localized around the

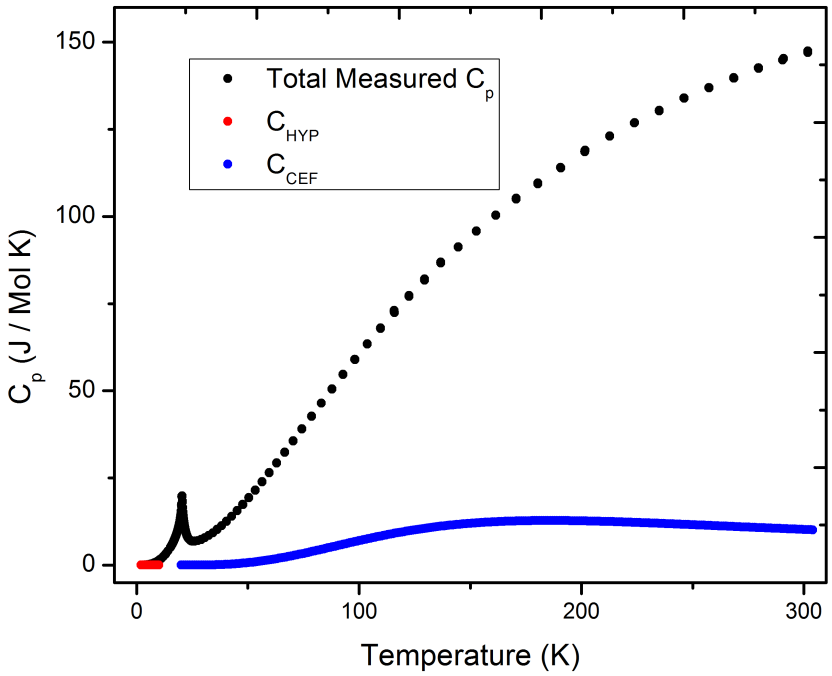

Figure 5.5: Comparrisson of specific heat contributions in parent CGO. The hyperfine contribution is small and is only important at very low temperatures (at $T = 5K$ $C_{hyp} = 5.64 \times 10^{-5}$ J/mol$_{CGO}$K). Above 20 K specific heat caused by crystal electric field transitions becomes substantial (at $T = 187$ K $C_{CEF} = 12.77$ J/mol$_{CGO}$K).

transition temperature and is negligible at high temperature. To isolate C_{mag}, the lattice contribution must be determined and subtracted. A common approach is to use a T^3 Debye term at low temperatures. [68, 7] This analysis requires high quality low temperature data and simultaneous fitting above T_N to accurately determine the lattice contribution. Furthermore, below T_N there is a magnetic transition in CGO, so that one must include a gapped spin wave term [7] which will have an unknown response to Mg^{2+} substitution. To simplify the analysis in light of these difficulties the Padé approximant method [69] which was used in Chapter 4. The benefit of this method is that temperatures sufficiently far away from the magnetic transition are used in the fit to determine C_{lat}. Thus, one only needs to include the lattice contribution as the magnetic contribution is assumed to be negligible. Specifically for $GeCo_{2-x}Mg_xO_4$, the temperature range of 90 K to 300 K was

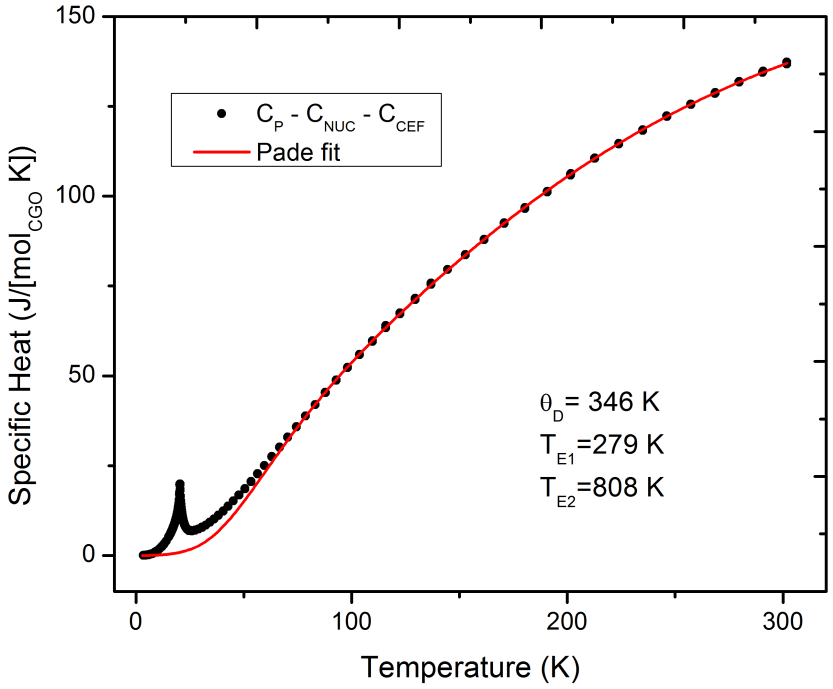

Figure 5.6: Padé fit to specific heat data which has been corrected for hyperfine and crystal electric field contributions. The data was fit over the range of 90K to 300K and extrapolated down to 2 K.

used which requires the inclusion of Einstein terms to describe the optical modes such that

$$C_{lat} = AC_{pade} + BC_{E1} + CC_{E2} \tag{5.5}$$

where, similar to NGO, C_E is given by equation 4.4 and A+B+C=7. Results of this analysis for the parent compound are illustrated in Figure 5.6 where the Padé fit was extrapolated back to 2 K. The fit values obtained $\Theta_D = 346$ K, $T_{E1} = 279$ K, and $T_{E2} = 808$ K compare favourably to results from NGO, found in Chapter 4, where $\Theta_D = 344$ K, $T_{E1} = 491$ K, and $T_{E2} = 826$ K. The Debye temperature determined here is smaller than the value obtained by Lashley*et al* ($\Theta_D = 444$ K) [7]. This is possibly from differences in analysis technique. It is noteworthy that the specific heat analysis used here yields a value for magnetic entropy which is much closer to the theoretical value when compared to the value resulting from $\Theta_D = 444$ K (see Figure 5.9).

This procedure was repeated for $GeCo_{2-x}Mg_xO_4$ (x=0.05, 0.10, 0.15, 0.30,

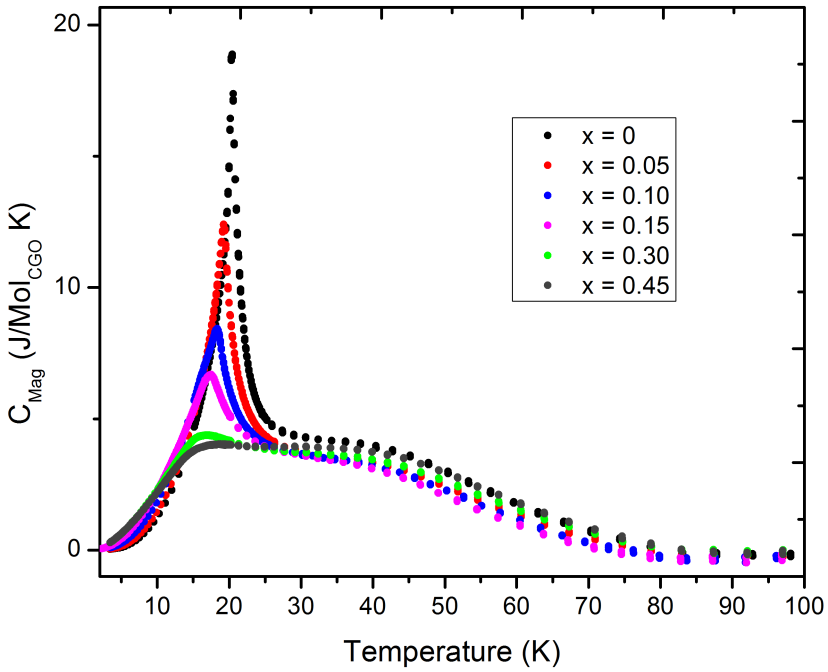

Figure 5.7: Magnetic specific heat of $GeCo_{2-x}Mg_xO_4$ (x=0.05, 0.10, 0.15, 0.30, 0.45).

0.45) to obtain the magnetic heat capacity by subtracting the contribution from C_{lat}. An illustration of the results is found in Figure 5.7. The parent compound undergoes a magnetic transition characterized by ferromagnetic order within similar planes and AFM order between similar planes, all of which occurs simultaneously. [5] This simultaneity may arise due to stronger inter-planar coupling in CGO compared to NGO. [37] The effect of magnetic dilution on these simultaneous transitions to an LRO state appears to retain this feature,that is, the transition is not split into two separate transitions with increased dilution. As Mg^{2+} concentration is increased, the peak occurs at lower temperatures and broadens which is an indication of a shift to short ranged order. In addition, a distinct maximum is observed until $x = 0.15$ (7.5 %) which suggests that the ordered state in CGO is more robust to dilution than NGO which loses its well defined maximum at approximately $x = 0.05$ (2.5 %). Another noticeable feature is a shoulder above the magnetic transition from approximately 30 K to 80 K that is present for all samples measured. One possible explanation for this are the spin wave

excitations which have a gap of 38 K. If this interpretation is correct, it would indicate that the spin wave gap exists for materials with 22 % of magnetic ions removed.

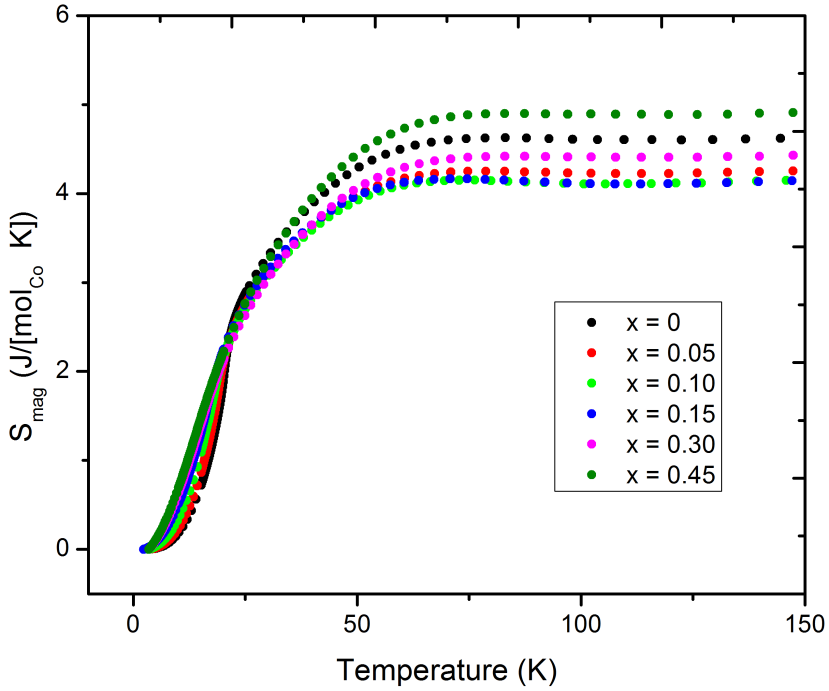

Figure 5.8: Magnetic entropy vs Temperature of $GeCo_{2-x}Mg_xO_4$ (x=0.05, 0.10, 0.15, 0.30, 0.45).

It is clear from Figure 5.7 that the magnetic specific heat peak broadens and reduces in temperature. Physically, this results from slow destruction of the LRO state due to the random placement of non-magnetic Mg^{2+} ions which perturbs the magnetic exchange network. A quantitative measure of this disorder is the magnetic entropy which can be calculated by

$$\Delta S = \int_a^b \frac{C(T)}{T}\,\mathrm{d}T. \tag{5.6}$$

To compare diluted samples with one another, the entropy change per mole of Co^{2+}, referenced from $T = 3$ K, was calculated and is displayed in Figure 5.8. The following three features are immediately apparent, namely, there exists a crossover temperature for all samples, secondly, diluted samples have

a greater magnetic entropy increase below the cross-over temperature, and thirdly, all samples have a maximum magnetic entropy change at approximately 75 K. The theoretical magnetic entropy should have a value given by $2R\ln(2J+1)$ where $J = 1/2$ in CGO. This gives an expected value of 11.53 J/mol$_{\mathrm{CGO}}$K which compares favourably with the calculated value of 9.25 J/mol$_{\mathrm{CGO}}$K at $T = 78$ K (80 % of the expected magnetic entropy). Furthermore, in the parent compound 4.30 J/mol$_{\mathrm{CGO}}$K (46 %) is recovered below T_N. This is in contrast to the results of Lashley *et al* where only 58.3 % is recovered between 2 and 75 K. [7]

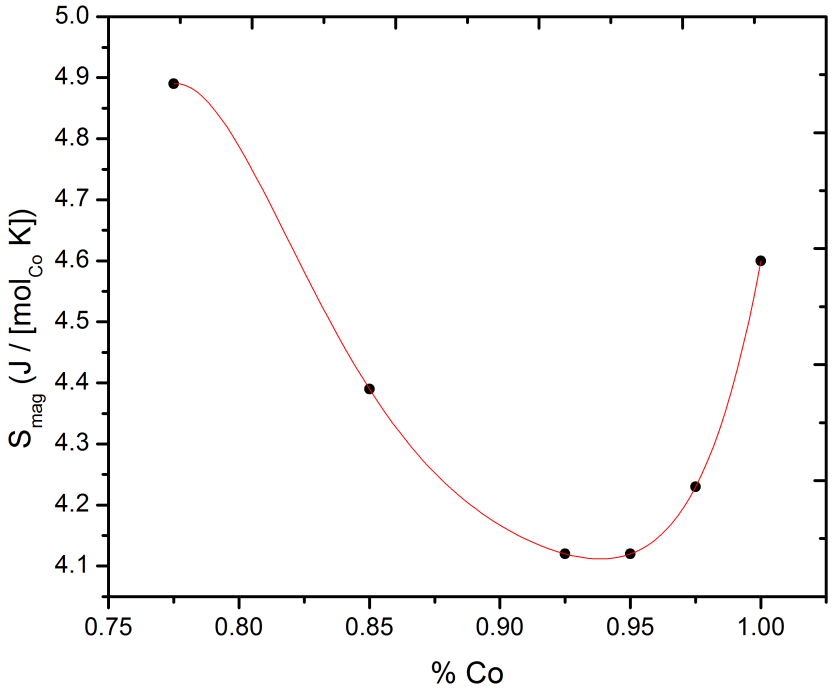

Figure 5.9: Magnetic entropy versus Co^{2+} concentration for $GeCo_{2-x}Mg_xO_4$. The red line is a guide for the eye.

To better observe the effects of magnetic dilution on the maximum magnetic entropy change, a plot of ΔS with respect to Co^{2+} concentration is found in Figure 5.9. The parent CGO compound exhibits a ΔS of 4.6 J/mol$_{Co}$K with a steady decrease to a minimum value of 4.11 at a Mg^{2+} concentration of 6%. The value of ΔS matches the value for the parent material at an estimated dilution level of 18 % which is near the concentration where a well

defined maximum in C_{mag} qualitatively disappears at x= 0.30 (15 %). This is, as will be argued below, the concentration at which spin glass behaviour emerges.

5.1.4 AC Magnetization

To further probe the nature of the low temperature magnetic state of moderately diluted compounds, AC susceptibility measurements were completed. In section 5.1.3, with increased dilution, the magnetic specific heat became highly broadened and lost its distinct maxima. The DC susceptibility in section 5.1.2 suggests the onset of spin glass freezing due to the presence of relaxation time scales. The shift to a spin glass low temperature state can be determined by analysing the AC susceptibility for signatures of spin freezing, specifically, a sudden jump in the imaginary component $\chi^{''}$, a cusp in the real component $\chi^{'}$, and frequency dependence in the freezing temperature T_f. [17]

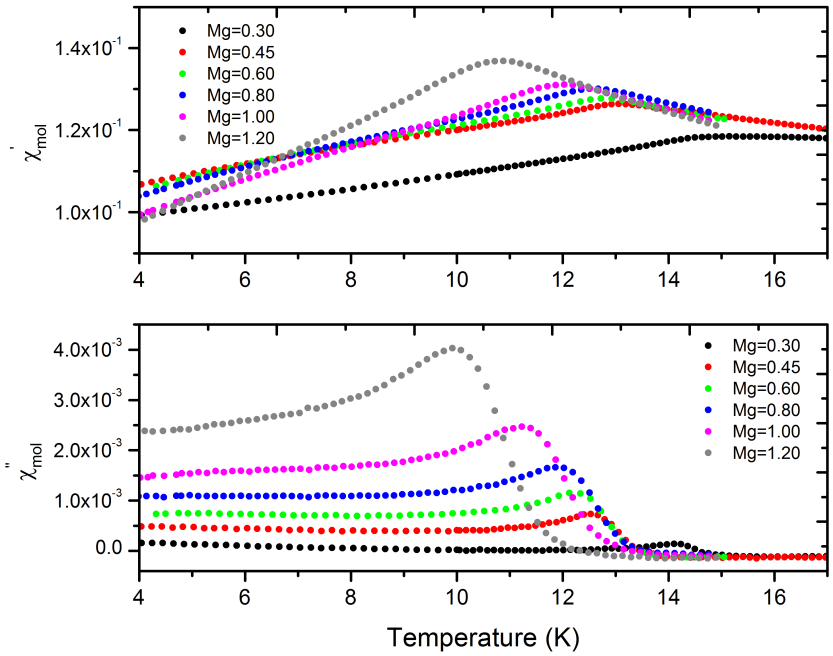

Figure 5.10: AC susceptibility data for several diluted values of $GeCo_{2-x}Mg_xO_4$ taken at 1000 Hz. The top graph is the real component $\chi^{'}$, the bottom is the imaginary component.

The AC magnetic susceptibility data for $GeCo_{2-x}Mg_xO_4$ (x = 0.30 to 1.2) is illustrated in Figure 5.10. The first two characteristics of a spin glass freezing transition are immediately present, namely, a jump in $\chi^{''}$ from a zero to non-zero value and a corresponding symmetric cusp in $\chi^{'}$. In addition, there is an observed frequency dependence on the freezing temperature.

This behaviour, combined with broad features in the magnetic heat capacity, indicate that $GeCo_{2-x}Mg_xO_4$ has a spin glass low temperature state when x $\geq$ 0.30.

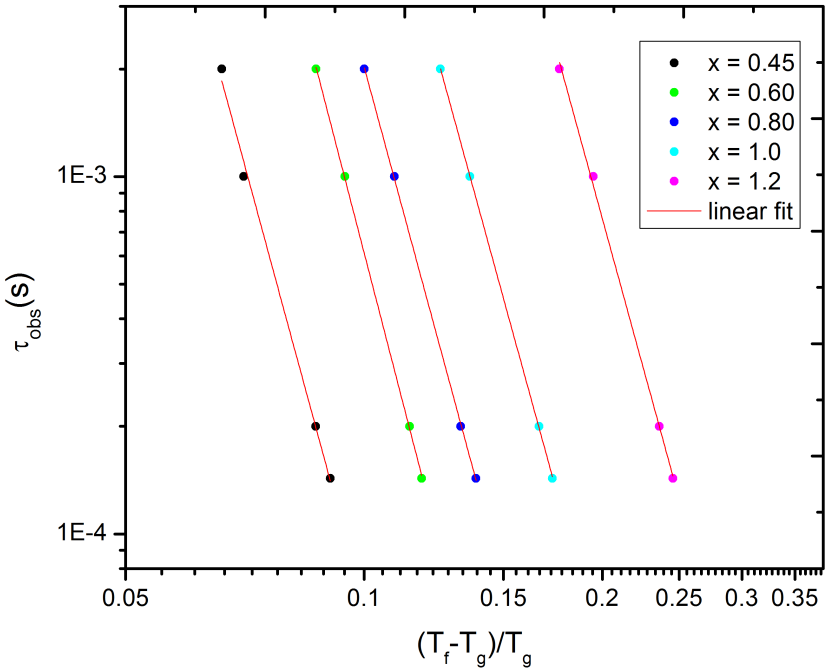

Figure 5.11: Plot of Frequency dependence of spin glass freezing temperature of $GeCo_{2-x}Mg_xO_4$.

The frequency dependence of T_f can be quantified to compare the spin glass state to the related compound $GeNi_{2-x}Mg_xO_4$ which, as described above, exhibits SG behaviour when x $\geq$ 0.30 (see section 4.1.4). Using equation 2.8, the values of $\sigma(x)$, where x is Mg^{2+} stoichiometry, are found to be the following: 0.0077, 0.0087, 0.011, 0.013, 0.016, 0.022 for x = 0.30, 0.45, 0.60, 0.80, 1.0, and 1.2, respectively. These values indicate an increasing trend that grows with higher dilution and are larger than the $\sigma(x)$ values obtained for diluted NGO. A greater frequency dependence (larger $\sigma(x)$) has been shown to be indicative of strong spin interactions. [17, 70] Stronger spin interactions are expected for CGO, compared to NGO, as a possible explanation for simultaneous ordering of kagomé and triangular planes. [7, 37] The frequency dependence can also be fit to the power law expression given in equation 2.11 to determine the characteristic relaxation time τ_* and the prod-

Table 5.1: Summary of spin glass data for $GeCo_{2-x}Mg_xO_4$

Dilution (%)	$z\nu$	$\tau_*(10^{-13}s)$	T_f (K)
22.5	8.2 ± 0.3	4 ± 3	11.99
30	8.56 ± 0.09	17.0± 4	11.45
40	8.18 ± 0.07	130 ± 20	11.06
50	8.08 ± 0.05	1020 ± 90	10.24
60	8.1 ± 0.2	17000 ± 500	8.71

uct of the dynamic and correlation length critical exponents zν. This fit is shown in Figure 5.11 and the results are summarized in Table 5.1. The values for the critical exponent product zν appear to be concentration independent and lie in the range 6 - 12 found for several SG systems. [55, 87] Contrasting this is τ_* which has a strong dilution dependence that increases with Mg^{2+} concentration. For canonical spin glasses, the value of τ_* is approximately 10^{-12} to 10−14. [88, 56] For cluster glasses, where groups of weakly interacting large spin clusters flip, the value is larger.[51] Due to the large increase in relaxation time τ_* from 4×10^{-13} to 1.7×10^{-9}, CGO appears to transition from a canonical spin glass to a cluster glass with increased Mg^{2+} dilution.

5.1.5 Pressure Effects

As described in the introduction, $GeCo_2O_4$ undergoes two structural distortions, firstly, at the AFM ordering temperature there is a small change in cubic cell volume, and secondly, at T=16K there is structural transition from cubic to tetragonal. The cubic-tetragonal transition results in a simultaneous increase in lattice parameter c and decrease in lattice parameter a, resulting in an overall reduction of unit cell volume by approximately 0.01 %. [43] The magnetic susceptibility for several applied pressures was measured over a temperature range of $T = 15$ K to 25 K. The results are illustrated in Figure 5.12. Regarding the structural transition at 16 K, there was no anomaly detected at any of the applied pressures. There is a measured increase in T_N which may be explained by the subtle decrease in cubic unit cell volume at ambient pressures during magnetic ordering. One can view the applied pressure reducing the unit cell size possibly making AFM more energetically favourable to occur at slightly higher temperatures.

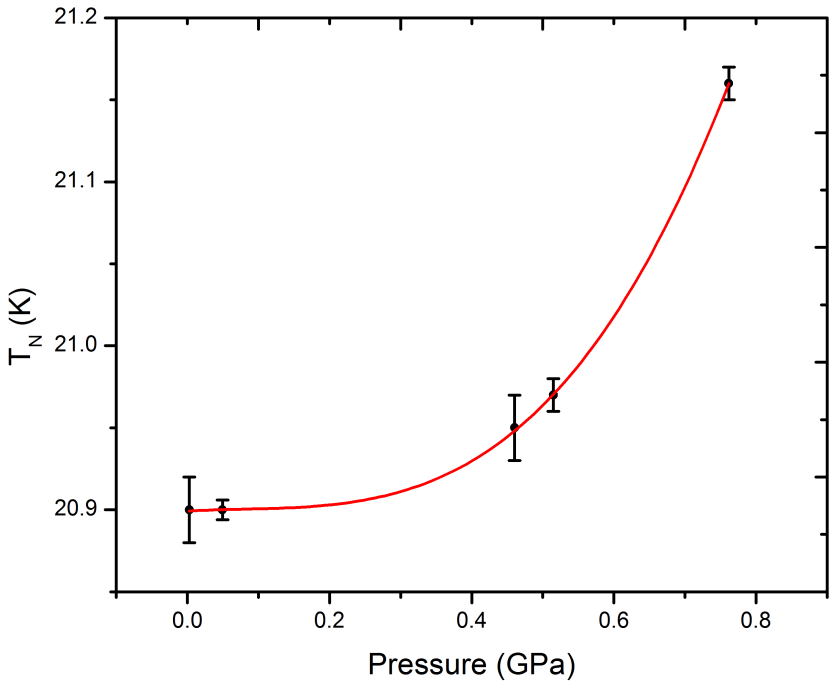

Figure 5.12: Plot of Néel temperature dependence of $GeCo_2O_4$ due to the effects of quasi-hydrostatic pressure. The solid line is a guide for the eye.

This pressure response is contrasted to NGO where there is a decrease in both ordering temperatures. In addition, the response in NGO is linear while the effects are highly non-linear in CGO. These differences are unexpected as magneto-restriction occurs in both materials at their respective ordering temperatures. The difference in pressure response may be due to magneto-dielectric coupling, which is distinct in CGO, that occurs at T_N. [43] Dielectric measurements by Barton *et al* have found a sharp drop in dielectric constant at T_n that is field dependent. Careful analysis of the dielectric constant suggests that coupling to an optical phonon mode at 303 cm^{-1} may be responsible for this behaviour. The pressure effects on this mode, which is intricately connected to the magnetism in CGO, may be the root of the difference in pressure response between CGO and NGO.

5.2 Discussion

Compiling all of the transition temperature measurements from AC and DC susceptibility data allows the construction of the proposed dilution phase diagram given in Figure 5.13. The demarcation line from an AFM to spin glass low temperature state is set at x = 0.30 due to the onset of a non-zero jump in the imaginary AC susceptibility $\chi^{''}$. However, it was not possible to determine accurate freezing temperatures, by calculation of maxima in $\chi^{'}$ or minima in $d\chi^{''}/dT$ as done in the other SG samples, due to how subtle the features were. In addition, the magnetic heat capacity peak has a broad maxima occurring at approximately 17.0 K; nearly 3 K higher than the AC susceptibility feature. This differential is a common characteristic in spin glasses [16, 10] and is further evidence for the glassy nature of $GeCo_{1.7}Mg_{0.3}O_4$. This behaviour, combined with its small features, suggests that the onset of SG behaviour occurs approximately at x=0.30. In the remainder of this section the Néel and SG regions will be discussed in greater detail.

5.2.1 Low Dilution (x < 0.30)

The effects of magnetic dilution on the layered magnetic ground state of $GeCo_2O_4$ appear to evolve in a well defined linear fashion. To estimate the percolation threshold, the steady decrease in T_N with respect to dilution parameter x was extrapolated to $x_c = 1.10$. Using the same methodology described in 4.2.1, the critical percolation threshold was estimated at $p_c = 0.45$. This value compares favourably to the theoretical values give in Table 2.1 such as the B-site Spinel ($p_c = 0.39$) and pyrochlore slab ($p_c = 0.50$). However, because CGO has a large exchange network of up to J_4, it is surprising that an experimental threshold of 0.448 is obtained. Increasing the number of neighbours (connectivity) decreases the percolation threshold. [47] Despite this, p_c for diluted CGO bares striking resemblance to $ZnCr_{2-2x}Ga_{2x}O_4$, which has a percolation threshold of approximately 0.50, when extrapolated in the same fashion as described above. [89] However, a more fruitful comparison to CGO can be drawn from diluted NGO, both of whose parent compounds share an identical ordered magnetic state.

In NGO, magnetic dilution produces anomalous percolation thresholds that are extremely high given its dimensionality and connectivity. This is not the case in diluted CGO in spite of their respective parent compounds sharing

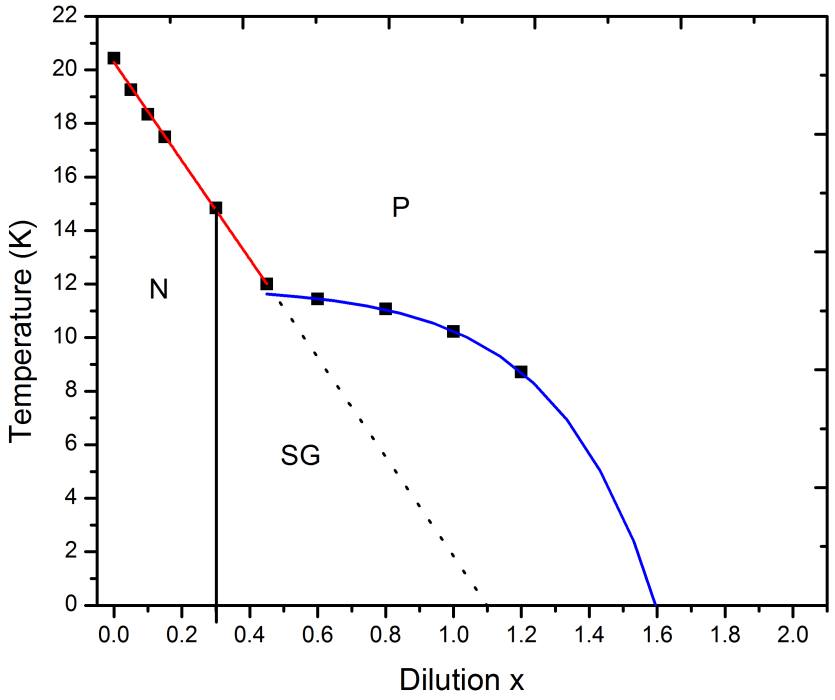

Figure 5.13: Proposed phase diagram of $GeCo_{2-x}Mg_xO_4$ (N = Néel order, SG = spin glass, P = paramagnetic). The dashed line is a linear extrapolation to to determine the percolation threshold. The solid blue line is a guide for the eyes.

many similarities. For example, besides exhibiting the same magnetic ground state, the exchange network of up to J_4 exists in both systems (although CGO has an additional FM direct exchange term). [5] In addition, both materials undergo a slight unit cell shrinkage at their respective ordering temperatures. [43]

The simultaneous ordering behaviour of the kagomé and triangular planes appears to remain in diluted CGO samples. That is, there is no evidence in any of the bulk probes used to indicate that the ordering of kagomé and triangular planes becomes decoupled with increasing Mg concentrations. If it did occur, there would be some observable anomaly at a separate temperature that would indicate this shift. This is an interesting feature in light of the similarities to NGO, which does have separate planar ordering temperatures that are exacerbated by the effects of dilution.

5.2.2 Spin Glass ($0.30 \leq x \leq 1.20$)

Similar to the related compound NGO, the spin glass state of CGO develops without glassiness occurring on distinct planes at distinct temperatures. However, given that CGO maintains the simultaneous ordering of kagomé and triangular planes, it is not very surprising. One feature that is rather striking is the transition from a canonical spin glass with $\tau_* = 4 \times 10^{-13}$ s (approximately the spin-flip time of single atomic moment [88]) to a cluster glass with $\tau_* = 1.7 \times 10^{-9}$ s. [51, 56] A possible explanation for this effect is that as spin glass form of CGO is further diluted, the magnetic network becomes more fractured. As a result, there is a greater number of unconnected clusters of spins that are weakly coupled. The effect of this would be that the fluctuating entities become larger and larger groups of spins (clusters) which would result in a larger τ_*. Large values of this size are observed in systems of nano-sized amorphous Fe_2O_3 which behave like a spin glass of small weakly interacting clusters. [56]

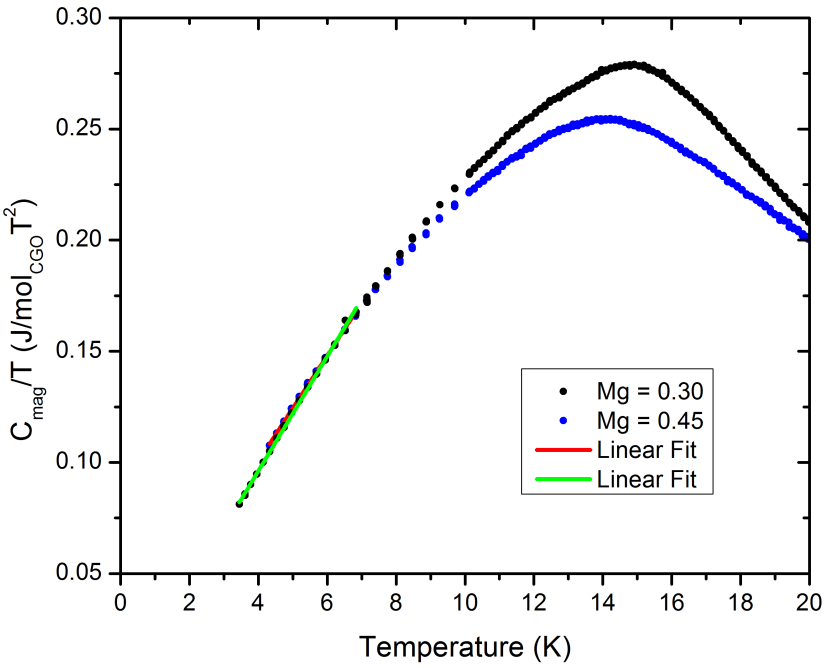

Figure 5.14: Linear fit to low temperature Specific heat of spin glass $GeCo_{2-x}Mg_xO_4$ (x=0.30, 0.45).

Furthermore, upon closer inspection of the low temperature behaviour

of the magnetic heat capacity for CGO in the spin glass regime, there is a clear proportionality to T^2. The data and linear fits for $GeCo_{2-x}Mg_xO_4$ (x=0.30, 0.45) are given in Figure 5.14. This is highly unusual for spin glass compounds as $C_{mag} \sim T$ is understood as canonical behaviour. [16] Other systems also have been found to exhibit T^2 behaviour in the low temperature magnetic heat capacity, such as $Ni_{2-x}Mg_xGeO_4$, deuteronium jarosite $(D_3O)Fe_3(SO_4)_2(OD)_6$ [78], and SCGO(x). [33] For the latter two, it has been shown that the quadratic magnetic heat capacity stems from a 2 dimensional character of the spin glass.

5.3 Conclusion

The effects of magnetic dilution and applied pressure on $GeCo_{2-x}Mg_xO_4$ are studied by measuring the DC magnetization, specific heat, and AC susceptibility for samples with $x = 0$ to 1.2. The goal of this work was to better understand how perturbations are manifested on the long distance exchange network of CGO. Furthermore, due to the similarities described above with $GeNi_{2-x}Mg_xO_4$ which exhibits 2 distinct magnetic transitions and anomalous percolation properties, CGO acts as a form of "control" to compare to. The results indicate that diluted CGO has two low temperature ground states, namely, AFM ordered ($x < 0.30$) and spin glass ($0.30 \leq x \leq 1.20$).

In the low dilution regime, there is a steady decrease in ordering temperature with increased non-magnetic Mg^{2+} concentration. Extrapolating the percolation threshold for the system yields $p_c = 0.448$, which is higher than expected for a 3 dimensional system with exchange interactions up to J_4. However, this value is far more reasonable than the values obtained for diluted NGO. Due to the similarities between the two systems, it is possible that the anomalous percolation threshold values for NGO stem from the coupling of kagomé and triangular networks that order independently in NGO. In this respect, CGO acts as a control for structure, the exchange network size and magnetic ground state as they are common to both systems. Furthermore, bulk probe measurements indicate that CGO in this dilution range maintains the simultaneous ordering of the kagomé and triangular planes. This is an interesting result considering that in NGO under increasing dilution, it appears that the triangular planes quickly became disordered while the kagomé planes slowly evolve into a spin glass.

For dilution levels greater or equal to 0.30, CGO behaves as a spin glass.

There is no bulk probe evidence for two distinct glass phases that correspond to the kagomé network or triangular network. Analysis of the frequency dependence of the SG freezing temperature indicates a possible dilution driven transition from a canonical to cluster spin glass. Evidence for this behaviour lies in the systematic increase τ_* from $7 \times 10^{-}13$ to 1.7×10^{-9}. These time scales are characteristic of single atomic moment flips, and spin clusters in nanosized Fe_2O_3, respectively. [56] Lastly, low temperature magnetic specific heat data is proportional to T^2 which is characteristic of 2D spin glass systems. Therefore, it suggests that there is a shift from from a 3 dimensional LRO state to 2 dimensional spin glass state which is driven by the quenched disorder of random non-magnetic Mg^{2+} placement.

Chapter 6

Frustrated $Ni_{1-x}Mg_xAl_2O_4$

6.1 Results

6.1.1 DC Magnetization

In $NiAl_2O_4$ (NAO) the Ni^{2+} ions reside in the diamond type sub-lattice that is associated with the A-sites in the spinel structure (see Figure 1.2b). In this arrangement, the Ni^{2+} ions are in tetrahedral coordination with the surrounding O^{2-} anions. This crystal field environment, coupled with spin-orbit interactions, split the degenerate 3d levels which yields a low lying S=1 level. [90] The Al^{3+} ions that reside on the B-sites only have a diamagnetic contribution to the total magnetism of the compound. Low temperature DC susceptibility results for $NiAl_2O_4$ are illustrated in Figure 6.1. Before any analysis was undertaken, the diamagnetic and temperature independent paramagnetism (TIP) was accounted for. An estimate for the diamagnetic susceptibility was obtained by adding the individual Ni^{2+}, Al^{3+}, and O^{2-} ion contributions found in Selwood. [91] This resulted in a value of $\chi_{dia} = 6.4 \times 10^{-5}$ $cm^3mol^{-1}_{NAO}$. The TIP contribution was calculated using equation 4.1 where Δ is the energy splitting between the lowest electronic level and first excited level. [63] A value of 8.0×10^{-4} $cm^3mol^{-1}_{NAO}$ was estimated using $\Delta =$ 5,000 cm^{-1}. With these contributions subtracted, the standard Curie-Weiss analysis could be performed on the inverse susceptibility. The linear fit of χ^{-1} was restricted to the temperature range above 100 K due to substantial non-linearities below this temperature. Results from inverse susceptibility analysis yield a Curie-Weiss temperature of 22.5 ± 0.9 K and Curie constant $C = 1.340 \pm 0.003$ ($cm^3mol^{-1}_{NAO}K^{-1}$). Close inspection of low temperature susceptibility data suggests spin glass freezing behaviour occurring at $T_f =$ 5.19 K, with an irreversible cusp in the ZFC mode as shown in Figure 6.2. The frustration parameter [9] for NAO is calculated to be $f = 4.3$ which is larger than $GeNi_2O_4$. [7]

Upon magnetic dilution of the Ni^{2+} with Mg^{2+} ions, there is a steady

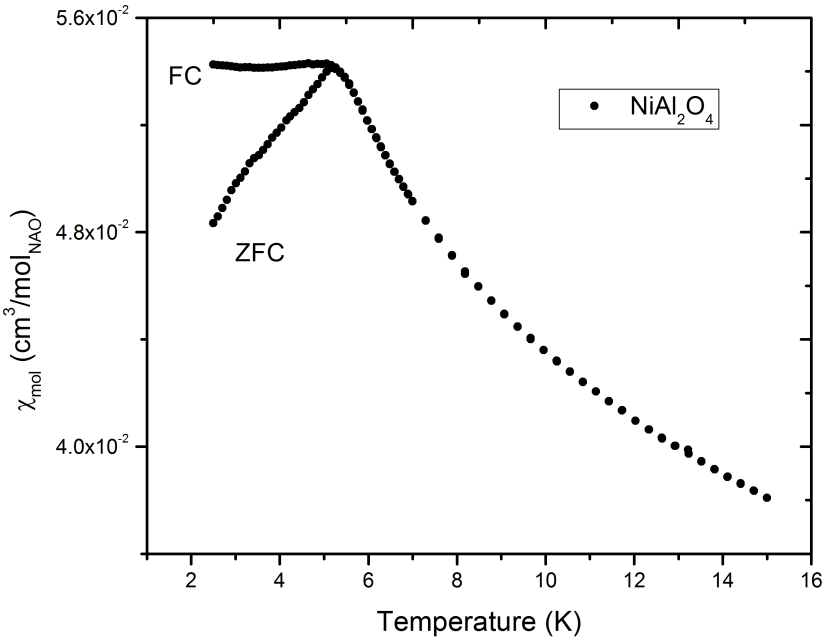

Figure 6.1: Molar magnetic susceptibility of $NiAl_2O_4$ in ZFC and FC mode.

decrease in the spin glass freezing temperature. Above x = 0.375, the freezing temperature is outside experimentally accessible temperatures (2.0 K). Linear extrapolation of the data yields a x = 0.66 for a freezing temperature of 0 K.

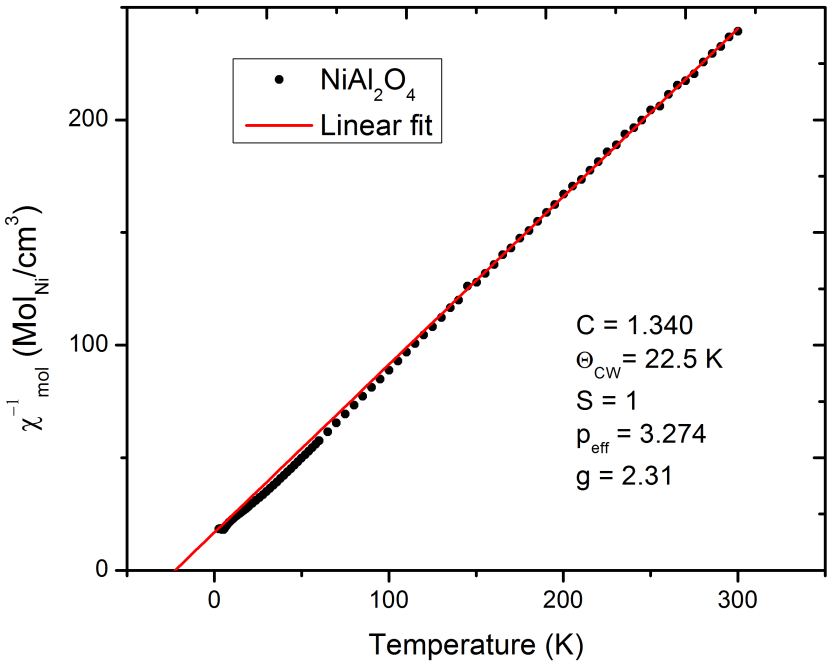

Figure 6.2: Inverse magnetic susceptibility of $NiAl_2O_4$. Linear fit is constrained to temperatures above 100 K as non-linearities occur below this value.

6.1.2 Specific Heat

To better understand the low temperature magnetic state, the heat capacity of $Ni_{1-x}Mg_xAl_2O_4$ (x = 0, 0.125) was measured. Just as in CGO and NGO, the total heat capacity can be decomposed into constituent contributions. Since NAO is an insulating oxide, the heat capacity from the conduction electrons is negligible and can be ignored. In addition, there are no hyperfine or crystal electric field state contributions. This stems from excited CEF levels being inaccessible at these temperature levels. Therefore, only the lattice and magnetic make a significant contribution to the specific heat. Thus, the analysis is the same as in Chapter 4 for NGO. The lattice contribution was modelled using equation 4.3 which contains a Debye term and two Einstein terms. Due to the broad anomaly at low temperatures, it is difficult to properly determine the Debye term using the low temperature T^3 form. To remedy this, the Padé approximant method was employed to determine the acoustic phonon contribution. This method allows one to fit a temperature

range which has negligible magnetic contributions (above 100 K). [69] The heat capacity data and resulting fit are illustrated in Figure 6.3.

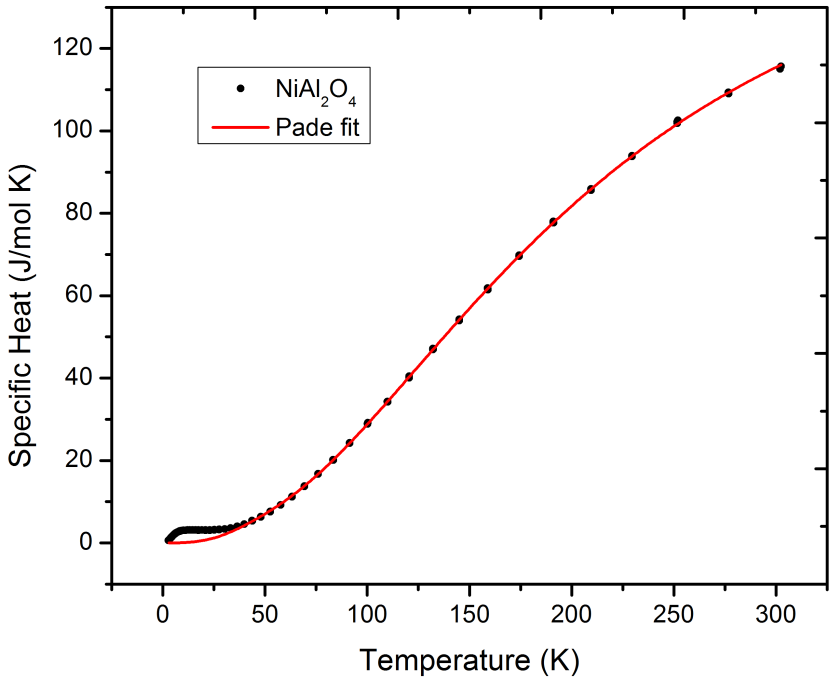

Figure 6.3: Specific heat of $NiAl_2O_4$. The Padé fit is constrained to the high temperature region of 100 K < T < 300 K.

The fit values obtained are $\theta_D = 331 \pm 6$ K, $T_{E1} = 519 \pm 4$ K, $T_{E2} = 894 \pm 4$ K for the Debye and Einstein temperatures, respectively. These values are comparable to other aluminate spinel compounds that have recently been studied. [29, 25] A summary of the results are given in table 6.2. The magnetic contributions can now be easily found and are displayed, for x = 0 and 0.125, in Figure 6.4. Both exhibit the same linear low temperature behaviour that is expected for canonical type spin glasses. [17, 10]

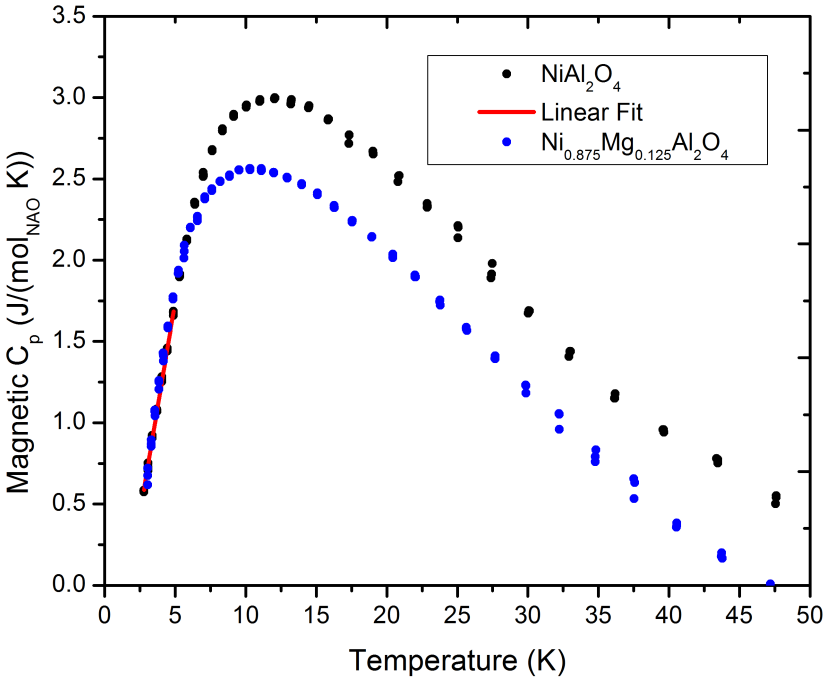

Figure 6.4: Magnetic specific heat contributions of $NiAl_2O_4$ (x = 0, 0.125). The low temperature linear fit establishes a linear relationship in C_{mag}.

6.1.3 AC Magnetization

To further characterize the low temperature magnetic data, one can probe the dynamics of the system through AC susceptibility measurements. AC data was taken for all samples, however, for $x = 0.5$ no transition is observed for experimentally accessible temperatures. The results are illustrated in Figure 6.5 and indicate the onset of spin glass behaviour. Specifically, there is a cusp in the real component $\chi^{'}$ and a sudden jump in the imaginary component $\chi^{''}$. The temperature at which these occur, has an observed frequency dependence. To compare this behaviour with other spin glass systems, the δ for each sample was calculated using equation 2.8. The values obtained for $\delta(x)$ are 0.0077, 0.0087, 0.011, 0.013 for $x = 0$, 0.125, 0.25, and 0.375, respectively. The parent, and samples with low levels of dilution ($x = 0$ to $x = 0.25$) have δ values that are characteristic of canonical type spin glasses with values ≈ 0.002. [57, 92] In materials with higher Mg^{2+} dilution, the frequency dependence increases to levels found in cluster spin glasses. In this

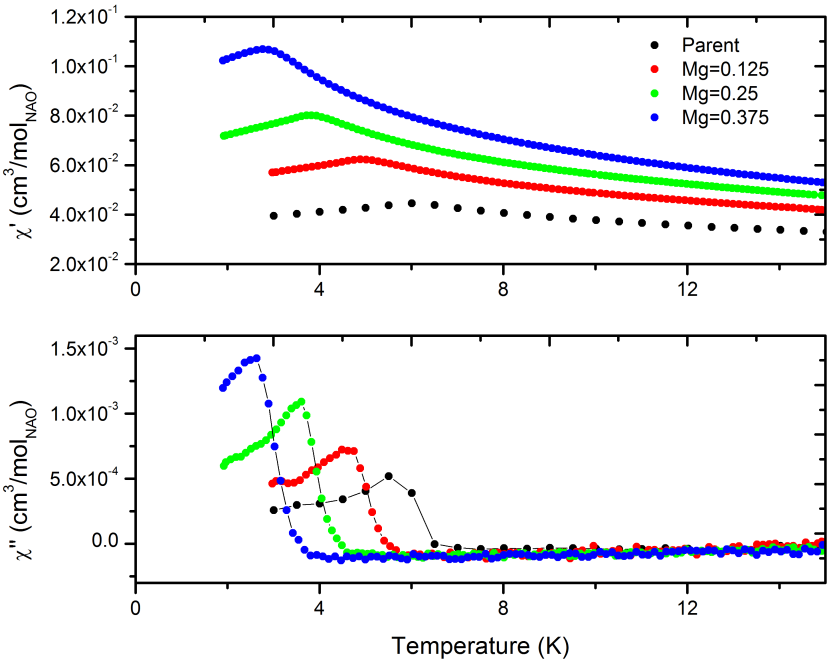

Figure 6.5: AC Susceptibility data for $Ni_{1-x}Mg_xAl_2O_4$ ($x = 0, 0.125, 0.25, 0.375$).

regime, the magnetic state is characterized by a collection of weakly interacting spin clusters and are interpreted as an intermediary between canonical glasses and superparamagnetism. [92, 51] This shift in δ was also observed in $GeCo_{2-x}Mg_xO_4$ and is discussed in Chapter 5. Similarly, these results suggest a shift from canonical to cluster glass behaviour due to the effects of random dilution. In the low dilution regime the magnetic network is still well connected and gives rise to canonical behaviour. At increased dilution levels, the network of magnetic Ni^{2+} sites becomes fractured and develops a system of weakly interacting clusters.

The frequency dependence can also be modelled using the power law found in equation 2.11. This is a more general result compared to the Arrhenius or Volger-Fulcher-Tamman forms, which have a more limited range of applicability. [55] The results of this analysis are illustrated in Figure 6.6 and summarized in Table 6.5. The values obtained for $z\nu$ and τ_* appear to be nearly uniform across all samples and average to 10.0 ± 0.5 and 4.6×10^{-13}, respectively. Both of these parameters fall within range of results

Table 6.1: Summary of AC data on $Ni_{1-x}Mg_xAl_2O_4$ samples.

Dilution (x)	$z\nu$	$\tau_*(10^{-13}s)$	T_f	δ
0	10.0 ± 0.1	3.2 ± 0.3	5.19	0.0077
0.125	9.3 ± 0.3	13 ± 4	4.24	0.0087
0.25	10.6 ± 0.2	1.6± 0.02	3.26	0.011
0.375	10.1 ± 0.1	1.0 ± 0.3	2.43	0.013

from canonical spin glasses. [55]

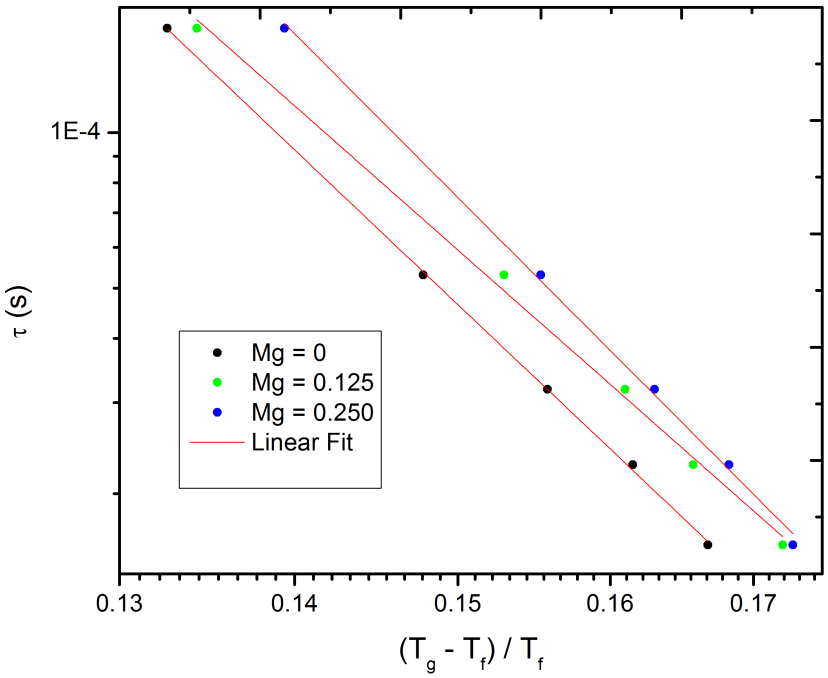

Figure 6.6: Power law fit to frequency dependence of the freezing temperatures in $Ni_{1-x}Mg_xAl_2O_4$.

Table 6.2: Comparrisson of data for $NiAl_2O_4$ and several aluminate spinel compounds.

Parameter	$NiAl_2O_4$	$CoAl_2O_4$	$FeAl_2O_4$	$MnAl_2O_4$
T_f	5.19	9.8	12.5	40.5
Θ_D	331	301	310	312
T_{E1}	519	530	563	522
T_{E2}	894	886	860	1092
f	4.3	22	11	3.6
p_{eff}	3.274	4.65	5.32	5.75
g_{eff}	2.31	2.40	2.17	1.94
Θ_{CW}	3.274	4.65	5.32	5.75
a	8.0486	8.1078	8.1572	8.2246

6.2 Discussion and Conclusion

A summary of data collected on $NiAl_2O_4$ with experimental data for $CoAl_2O_4$ [29, 25], $FeAl_2O_4$ [29], and $MnAl_2O_4$ [29] is found in Table 6.2. The Debye and Einstein temperature results for NAO are similar to the other materials listed. The effective g-factor of 2.31 in NAO is close to the spin only value of 2. Deviation from this value is also found in $GeNi_2O_4$ where $g_{eff} = 2.34$ and may stem from incomplete quenching of orbital angular momentum in Ni^{2+}. [7] It is interesting to note that NAO ($f = 4.3$), with no obvious triangular motifs, is more frustrated than NGO ($f = 1.3$).

The change in magnetic entropy $S(T) - S(T = 2.8)$ was determined from the magnetic specific heat and has a value of 5.9 $J/Mol_{NAO}K$. This is only 65 % of the total entropy expected for a system with $S(T = 0) = 0$. The remaining entropy and any zero-point entropy likely exist below 2.7 K which, unfortunately is outside experimental limits.

The true nature of the low temperature magnetic states of the aluminate compounds found in table 6.2 have been the subject of recent research. Specifically, the spin glass transition originally reported for $CoAl_2O_4$ by Tristan *et al.* has been suggested to be caused by site disorder due to small amounts of inversion of Co^{2+} and Al^{3+} ions. [25] Careful synthesis techniques produced $CoAl_2O_4$ samples with low levels of inversion and resulted in an antiferromagnetic transition at 9.8 K. [25] This synthesis procedure was also

completed on NAO, but did not result in a change in any of the physical properties. However, since this defect is so prevalent in all of the related aluminate spinels, and it destroys long range order in $CoAl_2O_4$, it is possible that defect free NAO has an AFM ground state.

Lastly, magnetic dilution of NAO does not have an appreciable effect on all of the quantities derived from specific heat and magnetic susceptibility data except for freezing temperature T_f and δ. The trend of increased δ values at great dilution levels, which is often used to estimate the relative interaction strength [51] between the SG building blocks (spins or clusters), suggests cluster glass development. However, analysis of the dynamic susceptibility yields a characteristic time $\tau_* \sim 10^{-13}$ that is the same order of magnitude of single atomic moments. [88] It remains unclear why evidence for cluster glass and canonical behaviour exist simultaneously in $Ni_{0.625}Mg_{0.375}Al_2O_4$. Further work on the aging behaviour of diluted NAO may help answer this question and determine the nature of the spin glass state.

Chapter 7

Conclusions

In this work, the effects of magnetic dilution and applied pressure on the magnetic networks found in $GeNi_2O_4$, $GeCo_2O_4$, and $NiAl_2O_4$ are studied. This is undertaken to better understand how the disorder, that is caused by random dilution, affects each sub-lattice that comprises the spinel-type structure. All three compounds crystallize in a spinel structure (AB_2O_4) which can be decomposed into two inter-penetrating sub-lattices. The A site sub-lattice has a diamond structure and the B sites form a structure found in pyrochlore sub-lattices. Motivation for this thesis stems from the unique low temperature magnetic state of $GeNi_2O_4$. In this compound, the kagomé and triangular planes order distinctly at $T_{N1} = 12.06$ and $T_{N2} = 11.54$ Kelvin, respectively. To generate this magnetic state, a long distance exchange network with strong J_4 interactions has been suggested. In light of the distinct magnetic ground state and long distance exchange network, the effects of dilution and applied pressure were studied.

The substitution of non-magnetic Mg^{2+} ions, in place of Ni^{2+} (S=1), in $GeNi_2O_4$ quickly destroys the long range order in the triangular planes when $x = 0.03$ (98.5 % Ni). Disorder in the kagomé planes quickly follows at dilution levels of $x = 0.05$ (97.5 % Ni). The percolation threshold for both sub-lattices are estimated to be $p_{c1} = 0.74 \pm 0.04$ and $p_{c2} = 0.65 \pm 0.5$ for the triangular and kagomé planes, respectively. These values are much larger than expected for the respective stacked planes. Effects from geometric frustration should not be significant as NGO has a low frustration parameter ($f = 1.3$). Also, there are no structural transitions which could result in an increase in p_c. A possible explanation is that the crystographically distinct kagomé and triangular planes act as coupled networks often termed a network of networks (NoNs). NoNs comprised of couple square lattices have been theoretically shown to be very susceptible to disorder caused by dilution. This occurs because failures of sites (dilution) on individual networks cascade through the entire system due to internetwork coupling. In diluted NGO, this could be interpreted as the magnetic disorder due to Mg^{2+} ions in one planar

type causing disorder in the other.

At higher dilution levels in $GeNi_{2-x}Mg_xO_4$ (NMGO(x)), of $x = 0.30$ and greater, the system behaves as a spin glass. Magnetic relaxation and AC susceptibility data indicate that it has a canonical type of behaviour. However, low temperature magnetic heat capacity yields a T^2 dependence which suggests a 2 dimensional character. Therefore, in addition to the extreme fragility of NGO, the system appears to transition from a 3D to a 2D system.

In an attempt to isolate the effects of having two distinct ordering temperatures, a suitable magnetic system was required as a comparison. $GeCo_2O_4$ (CGO) was chosen at it shares the same magnetic ground state, and contains a similar exchange network to NGO. However, but both triangular and kagomé planes order simultaneously in CGO. In this material, the ordered AFM state is much more robust against dilution with an estimated percolation threshold of $p_c = 0.448$. This result is similar in size to many two dimensional lattices. NGO and CGO share many features such as ground state and exchange network, but differ in the simultaneity of their associated planar ordering events. One may argue that this result strengthens the interpretation of an NoN behaviour in NGO.

In addition, further dilution at or above 15% in CGO results in a spin glass state. However, unlike NGO, dynamic susceptibility results suggest a shift from canonical to cluster glass behaviour. Lastly, magnetic heat capacity data exhibit a T^2 dependency which indicates a possible 2D behaviour. Thus, the only substantive way the spin glass states differ for CMGO(x) and NMGO(x), aside from freezing temperature, is the cluster glass behaviour of CGO. This may arise due to the stronger spin coupling that is required in CGO for simultaneous ordering of kagomé and triangular planes.

Lastly, dilution of the A-site sub-lattice was investigated with $Ni_{1-x}Mg_xAl_2O_4$ (NMAO(x)). Susceptibility results yield a spin glass state for all dilution levels in the range ($x = 0$ to 0.5). The linear dependence in the magnetic specific heat capacity results for NMAO(x) is an example of canonical spin glass behaviour. However, this state, found in the parent compound, may be caused by the site inversion problems that plague the aluminate spinels. This issue was highlighted, for example, in $CoAl_2O_4$ where early experiments indicated a spin glass phase. Later, with careful synthesis that minimizes the inversion of Ni^{2+} with Al^{3+} ions, an AFM long range ordered state was found. Therefore, the spin glass low temperature state of $NiAl_2O_4$ may be caused by site inversion and may not be intrinsic to the system.

7.1 Future Work

To further test the possibility of an NoN effect in the solid state, one can look for other materials which contain distinct magnetic networks. Specifically, systems that contain more than one ordering event that occur in distinct regions of the material. A possible candidate for this is $GeMn_2O_4$.

In $GeMn_2O_4$, which has an olivine structure, there are three distinct magnetic phase transitions and it is believed that they contain two magnetic sub-systems. [93] By diluting the Mn^2 sites with Mg^{2+} and monitoring the magnetic transition temperatures, one can determine the robustness of each ordered phase, and possibly their percolation thresholds.

Lastly, the magnetic low temperature structure of NGO can be probed by not only affecting magnetic sites, but also by affecting the bonds between them. This aggressive perturbation could be achieved through the replacement of Ni^{2+} ions in NGO with Li^{1+}. To retain the electric balance, the oxygen stoichiometry must be adjusted ($GeNi_{2-x}Li_xO_{4-\sigma}$) and would perturb the Ni-O-Ni superexchange pathways. Through this, one can now determine the effects of bond and site dilution on the ordered magnetic structures found in NGO.

Appendix A

Heat Capacity Details

A.1 Addenda Measurements

To achieve adequate thermal coupling of the sample to the platform a small amount of apiezon N grease was used. One accounts for this contribution to the overall measured value by first measuring the platform and grease heat capacity which is stored as an addenda. Once the sample is affixed to the grease on the platform, the total heat capacity is measured and the addenda value is subtracted automatically by the PPMS software. Figure A.1 illustrates the addenda measurement for $GeNi_2O_4$ in the range of 2 to 180 K.

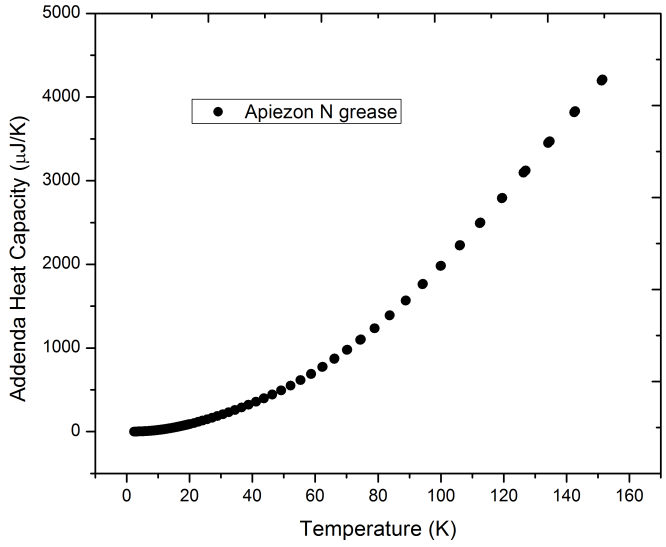

Figure A.1: Addenda measurement for $GeNi_2O_4$ in the temperature range of 2 to 180 K.

A.2 Characteristic Measurement Times

The PPMS heat capacity option utilizes a two tau method to determine the sample heat capacity. In all measurements the heating and cooling time constants, τ_1 and τ_2, were determine by the system automatically. For reference purposes, a plot of the heating time constant is plotted in Figure A.2.

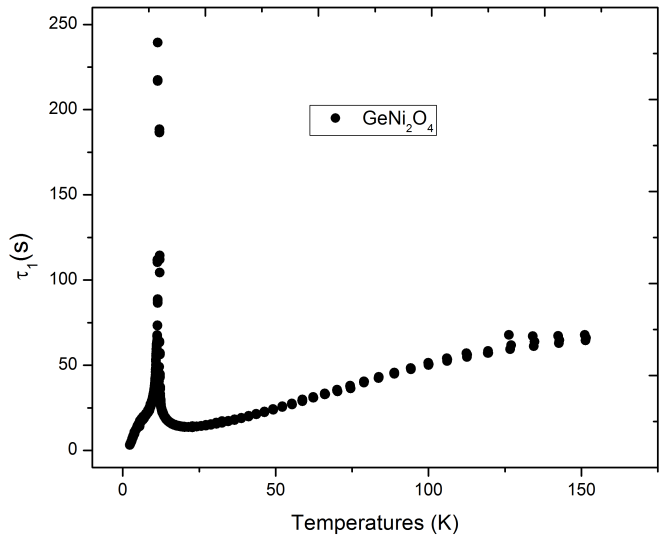

Figure A.2: Plot of heating characteristic time τ_1 for $GeNi_2O_4$.

Bibliography

[1] P.W. Anderson. *Basic Notions of Condensed Matter Physics*. Frontiers In Physics. Benjamin/Cummings Pub. Co., Advanced Book Program, 1984.

[2] Daniel L. Stein and Charles M. Newman. *Primers in Complex Systems*. Princeton University Press, 2013.

[3] M. Crawford, R. Harlow, P. Lee, Y. Zhang, J. Hormadaly, R. Flippen, Q. Huang, J. Lynn, R. Stevens, B. Woodfield, J. Boerio-Goates, and R. Fisher. Structure and Properties of the Integer-spin Frustrated Antiferromagnet $GeNi_2O_4$. *Physical Review B*, 68(22):220408, December 2003.

[4] Sébastien Diaz, Sophie de Brion, Michael Holzapfel, Gérard Chouteau, and Pierre Strobel. Study of Competitive Magnetic Interactions in the Spinel Compounds $GeNi_2O_4$, $GeCo_2O_4$. *Physica B: Condensed Matter*, 346-347:146–149, April 2004.

[5] S. Diaz, S. de Brion, G. Chouteau, B. Canals, V. Simonet, and P. Strobel. Magnetic Frustration in the Spinel Compounds $GeCo_2O_4$ and $GeNi_2O_4$. *Physical Review B*, 74(9):092404, September 2006.

[6] M Matsuda, J H Chung, S Park, T J Sato, K Matsuno, H Aruga Katori, H Takagi, K Kakurai, K Kamazawa, Y Tsunoda, I Kagomiya, C L Henley, and S H Lee. Frustrated minority spins in $GeNi_2O_4$. *EPL (Europhysics Letters)*, 82(3):37006, May 2008.

[7] J. Lashley, R. Stevens, M. Crawford, J. Boerio-Goates, B. Woodfield, Y. Qiu, J. Lynn, P. Goddard, and R. Fisher. Specific Heat and Magnetic Susceptibility of the Spinels $GeNi_2O_4$ and $GeCo_2O_4$. *Physical Review B*, 78(10):104406, September 2008.

[8] F. Scholl and K. Binder. Selective Sublattice Dilution in Ordered Magnetic Compounds: A New Kind of Percolation Problem. *Zeitschrift fr Physik B Condensed Matter*, 39(3):239–247, 1980.

[9] A P Ramirez. Strongly Geometrically Frustrated Magnets. *Annual Review of Materials Science*, 24(1):453–480, 1994.

[10] K.H. Fischer and J.A. Hertz. *Spin Glasses*. Cambridge Studies in Magnetism. Cambridge University Press, 1993.

[11] D. Stauffer and A. Aharony. *Introduction To Percolation Theory*. Taylor & Francis, 1994.

[12] P.D. Johnson, G. Xu, and W.G. Yin. *Iron-Based Superconductivity*. Springer Series in Materials Science. Springer International Publishing, 2015.

[13] I. Mirebeau, I. N. Goncharenko, P. Cadavez-Peres, S. T. Bramwell, M. J. P. Gingras, and J. S. Gardner. Pressure-induced Crystallization of a Spin Liquid. *Nature*, 420(6911):54–57, November 2002.

[14] Jason S. Gardner, Michel J. P. Gingras, and John E. Greedan. Magnetic Pyrochlore Oxides. *Rev. Mod. Phys.*, 82:53–107, Jan 2010.

[15] C. Lacroix, P. Mendels, and F. Mila. *Introduction to Frustrated Magnetism: Materials, Experiments, Theory*. Springer Series in Solid-State Sciences. Springer, 2011.

[16] K. Binder and A. P. Young. Spin Glasses: Experimental Facts, Theoretical Concepts, and Open Questions. *Rev. Mod. Phys.*, 58:801–976, Oct 1986.

[17] J A Mydosh. Spin Glasses: Redux: An Updated Experimental and Materials Survey. *Reports on Progress in Physics*, 78(5):052501, 2015.

[18] M. J. Harris, S. T. Bramwell, D. F. McMorrow, T. Zeiske, and K. W. Godfrey. Geometrical Frustration in the Ferromagnetic Pyrochlore $Ho_2Ti_2O_7$. *Phys. Rev. Lett.*, 79:2554–2557, Sep 1997.

[19] G. H. Wannier. Antiferromagnetism. The Triangular Ising Net. *Phys. Rev.*, 79:357–364, Jul 1950.

[20] J.A. Mydosh. *Spin Glasses: An Experimental Introduction*. Taylor and Francis, 1993.

[21] John E. Greedan. Geometrically Frustrated Magnetic Materials. *J. Mater. Chem.*, 11:37–53, 2001.

[22] R Moessner. Magnets with Strong Geometric Frustration. *Canadian Journal of Physics*, 79(11-12):1283–1294, 2001.

[23] Jurgen Schnack. Effects of frustration on magnetic molecules: a survey from olivier kahn until today. *Dalton Trans.*, 39:4677–4686, 2010.

[24] Rebecca Stevens, Brian F. Woodfield, Juliana Boerio-Goates, and Michael K. Crawford. Heat Capacities, Third-law Entropies and Thermodynamic Functions of the Geometrically Frustrated Antiferromagnetic Spinels $GeCo_2O_4$ and $GeNi_2O_4$ from T=(0 to 400) K. *The Journal of Chemical Thermodynamics*, 36(5):359–375, May 2004.

[25] B. Roy, Abhishek Pandey, Q. Zhang, T. Heitmann, D. Vaknin, D. Johnston, and Y. Furukawa. Experimental Evidence of a Collinear Antiferromagnetic Ordering in the Frustrated $CoAl_2O_4$ Spinel. *Phys. Rev. B*, 88:174415, Nov 2013.

[26] S.-H. Lee, C. Broholm, G. Aeppli, T. G. Perring, B. Hessen, and A. Taylor. Isolated Spin Pairs and Two-Dimensional Magnetism in $SrCr_{9p}Ga_{12-9p}O_{19}$. *Phys. Rev. Lett.*, 76:4424–4427, Jun 1996.

[27] C L Henley. Effective Hamiltonians and Dilution Effects in Kagomé and Related Anti-ferromagnets. *Canadian Journal of Physics*, 79(11-12):1307–1321, 2001.

[28] V. Fritsch, J. Hemberger, N. Büttgen, E.-W. Scheidt, H.-A. Krug von Nidda, A. Loidl, and V. Tsurkan. Spin and Orbital Frustration in $MnSc_2S_4$ and $FeSc_2S_4$. *Phys. Rev. Lett.*, 92:116401, Mar 2004.

[29] N. Tristan, J. Hemberger, A. Krimmel, H-A. Krug von Nidda, V. Tsurkan, and A. Loidl. Geometric Frustration in the Cubic Spinels MAl_2O_4 (M = Co, Fe, and Mn). *Phys. Rev. B*, 72:174404, Nov 2005.

[30] X. Obradors, A. Labarta, A. Isalgu, J. Tejada, J. Rodriguez, and M. Pernet. Magnetic Frustration and Lattice Dimensionality in $SrCr_8Ga_4O_{19}$. *Solid State Communications*, 65(3):189 – 192, 1988.

[31] B. Martínez, F. Sandiumenge, A. Rouco, A. Labarta, J. Rodríguez-Carvajal, M. Tovar, M.T. Causa, S. Galí, and X. Obradors. Magnetic Dilution in the Strongly Frustrated Kagomé Antiferromagnet $SrGa_{12-x}Cr_xO_{19}$. *Phys. Rev. B*, 46:10786–10792, Nov 1992.

[32] A. P. Ramirez, G. P. Espinosa, and A. S. Cooper. Strong Frustration and Dilution-enhanced Order in a Quasi-2D Spin Glass. *Phys. Rev. Lett.*, 64:2070–2073, Apr 1990.

[33] A. P. Ramirez, G. P. Espinosa, and A. S. Cooper. Elementary Excitations in a Diluted Antiferromagnetic Kagomé Lattice. *Phys. Rev. B*, 45:2505–2508, Feb 1992.

[34] A. Navrotsky and L. Hughes. Thermodynamic Relations Among Olivine, Spinel, and Phenacite Structures in Silicates and Germanates. *Journal of Solid State Chemistry*, 16(1-2):185–188, 1976.

[35] N.W. Ashcroft and N.D. Mermin. *Solid State Physics*. HRW international editions. Holt, Rinehart and Winston, 1976.

[36] T. Lancaster, S. Blundell, D. Prabhakaran, P. Baker, W. Hayes, and F. Pratt. Magnetism in the S=1 Frustrated Antiferromagnet $GeNi_2O_4$ Studied Using Implanted Muons. *Physical Review B*, 73(18):184436, May 2006.

[37] Masaaki Matsuda, Takemichi Hoshi, Hiroko Aruga Katori, Masashi Kosaka, and Hidenori Takagi. Magnetic-Field-Induced Transitions in Spinel $GeCo_2O_4$. *Journal of the Physical Society of Japan*, 80(3):034708, 2011.

[38] Rose M. Morra, William J. L. Buyers, Robin L. Armstrong, and K. Hirakawa. Spin Dynamics and the Haldane Gap in the Spin-1 Quasi-one-dimensional Antiferromagnet $CsNiCl_3$. *Phys. Rev. B*, 38:543–555, Jul 1988.

[39] M F Collins and O A Petrenko. Review: Triangular Antiferromagnets. *Canadian Journal of Physics*, 75(9):605–655, 1997.

[40] J. Takeuchi, T. Wada, I. Hiromitsu, and T. Ito. Magnetic Phase Transitions in Triangular-lattice Antiferromagnetic Mixed Crystals

$CsNi_{0.98}M_{0.02}Cl_3$ (M = Co, Fe, Mg) . *Solid State Communications*, 87(10):899 – 901, 1993.

[41] J R Stewart, G Ehlers, A S Wills, S T Bramwell, and J S Gardner. Phase Transitions, Partial Disorder and Multi- k Structures in $Gd_2Ti_2O_7$. *Journal of Physics: Condensed Matter*, 16(28):L321, 2004.

[42] H D Zhou, A Kiss, J A Janik, and C R Wiebe. Doping Through the Percolation Limit in $GeNi_{2-x}$ Co_xO_4. *Journal of Physics: Condensed Matter*, 19(15):156202, 2007.

[43] Phillip T. Barton, Moureen C. Kemei, Michael W. Gaultois, Stephanie L. Moffitt, Lucy E. Darago, Ram Seshadri, Matthew R. Suchomel, and Brent C. Melot. Structural Distortion Below the Néel Temperature in Spinel $GeCo_2O_4$. *Phys. Rev. B*, 90:064105, Aug 2014.

[44] S. Klemme and J.C. van Miltenburg. The heat capacities and thermodynamic properties of $NiAl_2O_4$ and $CoAl_2O_4$ measured by adiabatic calorimetry from T=(4 to 400) K. *The Journal of Chemical Thermodynamics*, 41(7):842 – 848, 2009.

[45] Nishimori and Ortiz. *Elements of Phase Transitions and Critical Phenomena*. Oxford University Press, 2011.

[46] M. Sahini and M. Sahimi. *Applications Of Percolation Theory*. Taylor & Francis, 1994.

[47] S. C. van der Marck. Percolation Thresholds and Universal Formulas. *Phys. Rev. E*, 55:1514–1517, Feb 1997.

[48] D. Fiorani, L. Gastaldi, A. Lapiccirrella, S. Viticoli, and N. Tomassini. Monte Carlo Simulation of Percolative Phenomena in the Cationic B-sublattice of Spinels. *Solid State Communications*, 32(9):831 – 832, 1979.

[49] K. Binder and W. Kob. *Glassy Materials and Disordered Solids: An Introduction to Their Statistical Mechanics*. World Scientific, 2011.

[50] R. V. Chamberlin, George Mozurkewich, and R. Orbach. Time Decay of the Remanent Magnetization in Spin-Glasses. *Phys. Rev. Lett.*, 52:867–870, Mar 1984.

[51] A. Malinowski, V. L. Bezusyy, R. Minikayev, P. Dziawa, Y. Syryanyy, and M. Sawicki. Spin-glass Behavior in Ni-doped $La_{1.85}Sr_{0.15}CuO_4$. *Phys. Rev. B*, 84:024409, Jul 2011.

[52] Gregg Lois, Jerzy Blawzdziewicz, and Corey S. O'Hern. Percolation Model for Slow Dynamics in Glass-Forming Materials. *Phys. Rev. Lett.*, 102:015702, Jan 2009.

[53] R. Bohmer, K. L. Ngai, C. A. Angell, and D. J. Plazek. Nonexponential Relaxations in Strong and Fragile Glass Formers. *The Journal of Chemical Physics*, 99(5):4201–4209, 1993.

[54] M. Alba, J. Hammann, M. Ocio, Ph. Refregier, and H. Bouchiat. Spin Glass Dynamics From Magnetic Noise, Relaxation, and Susceptibility Measurements (invited). *Journal of Applied Physics*, 61(8):3683–3688, 1987.

[55] J. Souletie and J. L. Tholence. Critical Slowing Down in Spin Glasses and Other Glasses: Fulcher Versus Power Law. *Phys. Rev. B*, 32:516–519, Jul 1985.

[56] M. D. Mukadam, S. M. Yusuf, P. Sharma, S. K. Kulshreshtha, and G. K. Dey. Dynamics of Spin Clusters in Amorphous Fe_2O_3. *Phys. Rev. B*, 72:174408, Nov 2005.

[57] J L Dormann, L Bessais, and D Fiorani. A Dynamic Study of Small Interacting Particles: Superparamagnetic Model and Spin-Glass Laws. *Journal of Physics C: Solid State Physics*, 21(10):2015, 1988.

[58] S. Shtrikman and E.P. Wohlfarth. The Theory of the Vogel-Fulcher Law of Spin Glasses. *Physics Letters A*, 85(8???9):467 – 470, 1981.

[59] A Eiling and J S Schilling. Pressure and Temperature Dependence of Electrical Resistivity of Pb and Sn from 1 - 300 K and 0-10 GPa. *Journal of Physics F: Metal Physics*, 11(3):623, 1981.

[60] Juan Rodrguez-Carvajal. Recent Advances in Magnetic Structure Determination by Neutron Powder Diffraction. *Physica B: Condensed Matter*, 192(12):55 – 69, 1993.

[61] A. R. Denton and N. W. Ashcroft. Vegard's Law. *Phys. Rev. A*, 43:3161–3164, Mar 1991.

[62] R. D. Shannon. Revised Effective Ionic Radii and Systematic Studies of Interatomic Distances in Halides and Chalcogenides. *Acta Crystallographica Section A*, 32(5):751–767, Sep 1976.

[63] Richard L. Carlin. *Magnetochemistry*. Springer-Verlag, 1986.

[64] Graham Williams and David C. Watts. Non-symmetrical Dielectric Relaxation Behaviour Arising From a Simple Empirical Decay Function. *Trans. Faraday Soc.*, 66:80–85, 1970.

[65] M.I. Klinger. *Glassy Disordered Systems: Glass Formation and Universal Anomalous Low-energy Properties*. World Scientific, 2013.

[66] M. A. Continentino and A. P. Malozemoff. Dynamic Scaling and the Field-Dependent Critical Line in a Fractal Cluster Model of Spin Glasses. *Phys. Rev. B*, 33:3591–3594, Mar 1986. MTRM.

[67] K. L. Ngai, A. K. Rajagopal, and C. Y. Huang. Relaxations in Spin Glasses: Similarities and Differences From Ordinary Glasses. *Journal of Applied Physics*, 55(6):1714–1716, 1984.

[68] E.S.R. Gopal. *Specific Heats at Low Temperatures*. International cryogenics monograph series. Plenum Press, 1966.

[69] R. J. Goetsch, V. K. Anand, Abhishek Pandey, and D. C. Johnston. Structural, Thermal, Magnetic, and Electronic Transport Properties of the $LaNi_2(Ge_{1-x}P_x)_2$ System. *Phys. Rev. B*, 85:054517, Feb 2012.

[70] Jean-Louis Tholence. Recent Experiments About the Spin-glass Transition. *Physica B+C*, 126(1???3):157 – 164, 1984.

[71] T. Hoshi, H. Aruga Katori, M. Kosaka, and H. Takagi. Magnetic Properties of Single Crystal of Cobalt Spinel. *Journal of Magnetism and Magnetic Materials*, 310(2, Part 2):e448 – e450, 2007. Proceedings of the 17th International Conference on Magnetism The International Conference on Magnetism.

[72] P. G. Reuvekamp, R. K. Kremer, J. Köhler, and A. Bussmann-Holder. Spin-lattice Coupling Induced Crossover From Negative to Positive Magnetostriction in $EuTiO_3$. *Phys. Rev. B*, 90:094420, Sep 2014.

[73] Anne M. Hofmeister. Calculation of Bulk Modulus and its Pressure Derivatives from Vibrational Frequencies and Mode Grneisen Parameters: Solids with Cubic Symmetry or One Nearest-neighbor Distance. *Journal of Geophysical Research: Solid Earth*, 96(B10):16181–16203, 1991.

[74] K. Fritsch, Z. Yamani, S. Chang, Y. Qiu, J. R. D. Copley, M. Ramazanoglu, H. A. Dabkowska, and B. D. Gaulin. Magnetic Order and Fluctuations in the Presence of Quenched Disorder in the Kagomé Staircase System $(Co_{1-x}Mg_x)_3V_2O_8$. *Phys. Rev. B*, 86:174421, Nov 2012.

[75] S. Havlin, D.Y. Kenett, A. Bashan, J. Gao, and H.E. Stanley. Vulnerability of Network of Networks. *The European Physical Journal Special Topics*, 223(11):2087–2106, 2014.

[76] Sergey V. Buldyrev, Roni Parshani, Gerald Paul, H. Eugene Stanley, and Shlomo Havlin. Catastrophic Cascade of Failures in Interdependent Networks. *Nature*, 464(7291):1025–1028, April 2010.

[77] Amir Bashan, Yehiel Berezin, Sergey V. Buldyrev, and Shlomo Havlin. The Extreme Vulnerability of Interdependent Spatially Embedded Networks. *Nature Physics*, 9(10):667–672, October 2013.

[78] A. S. Wills, A. Harrison, S. A. M. Mentink, T. E. Mason, and Z. Tun. Magnetic Correlations in Deuteronium Jarosite, a Model S = 5/2 Kagomé Antiferromagnet. *EPL (Europhysics Letters)*, 42(3):325, 1998.

[79] Andrew S. Wills and Andrew Harrison. Structure and Magnetism of Hydronium Jarosite, a Model Kagomé Antiferromagnet. *J. Chem. Soc., Faraday Trans.*, 92:2161–2166, 1996.

[80] C. A. M. Mulder, A. J. van Duyneveldt, and J. A. Mydosh. Frequency and Field Dependence of the AC Susceptibility of the AuMn spin-glass. *Phys. Rev. B*, 25:515–518, Jan 1982.

[81] C. A. M. Mulder, A. J. van Duyneveldt, and J. A. Mydosh. Susceptibility of the CuMn Spin-glass: Frequency and Field Dependences. *Phys. Rev. B*, 23:1384–1396, Feb 1981.

[82] K. Tomiyasu, M. K. Crawford, D. T. Adroja, P. Manuel, A. Tominaga, S. Hara, H. Sato, T. Watanabe, S. I. Ikeda, J. W. Lynn, K. Iwasa, and K. Yamada. Molecular Spin-orbit Excitations in the $J_{\text{eff}}=\frac{1}{2}$ Frustrated Spinel $GeCo_2O_4$. *Phys. Rev. B*, 84:054405, Aug 2011.

[83] Tadataka Watanabe, Shigeo Hara, Shin-Ichi Ikeda, and Keisuke Tomiyasu. Elastic Instabilities in an Antiferromagnetically Ordered Phase of the Orbitally Frustrated Spinel $GeCo_2O_4$. *Phys. Rev. B*, 84:020409, Jul 2011.

[84] J. Hubsch and G. Gavoille. First Order Magnetic Phase Transition in $GeCo_2O_4$. *Journal of Magnetism and Magnetic Materials*, 66(1):17 – 22, 1987.

[85] A. D. LaForge, S. H. Pulido, R. J. Cava, B. C. Chan, and A. P. Ramirez. Quasispin Glass in a Geometrically Frustrated Magnet. *Phys. Rev. Lett.*, 110:017203, Jan 2013.

[86] D. Bloch, J. Voiron, A. Berton, and J. Chaussy. The Hyperfine Specific Heat of $HoCo_2$. *Solid State Communications*, 12(7):685–687, April 1973.

[87] Andrew T. Ogielski. Dynamics of Three-dimensional Ising Spin Glasses in Thermal Equilibrium. *Phys. Rev. B*, 32:7384–7398, Dec 1985.

[88] C. L. S. Kantner, M. C. Langner, W. Siemons, J. L. Blok, G. Koster, A. J. H. M. Rijnders, R. Ramesh, and J. Orenstein. Determination of the Spin-flip Time in Ferromagnetic $SrRuO_3$ From Time-resolved Kerr Measurements. *Phys. Rev. B*, 83:134432, Apr 2011.

[89] S.-H. Lee, W. Ratcliff, Q. Huang, T. Kim, and S-W. Cheong. Néel to Spin-glass-like Phase Transition Versus Dilution in Geometrically Frustrated $ZnCr_{2-2x}Ga_{2x}O_4$. *Physical Review B*, 77(1):014405, January 2008.

[90] A. Abragam and B. Bleaney. *Electron Paramagnetic Resonance of Transition Ions*. Oxford Classic Texts in the Physical Sciences. OUP Oxford, 2012.

[91] P.W. Selwood. *Magnetochemistry*. Read Books, 2008.

[92] N. Marcano, J. C. Gomez Sal, J. I. Espeso, L. Fernandez Barquin, and C. Paulsen. Cluster-glass Percolative Scenario in $CeNi_{1-x}Cu_x$ Studied by Very Low-temperature AC Susceptibility and DC Magnetization. *Phys. Rev. B*, 76:224419, Dec 2007.

[93] N V Volkov, N V Mikhashenok, K A Sablina, O A Bayukov, M V Gorev, A D Balaev, A I Pankrats, V I Tugarinov, D A Velikanov, M S Molokeev, and S I Popkov. Magnetic Phase Diagram of the Olivine-type Mn_2GeO_4 Single Crystal Estimated From Magnetic, Resonance and Thermodynamic Properties. *Journal of Physics: Condensed Matter*, 25(13):136003, 2013.